Pharmacological induction of heat shock proteins ameliorates toxicity of mutant PKCγ in spinocerebellar ataxia type 14

Received for publication, March 13, 2018, and in revised form, July 26, 2018 Published, Papers in Press, August 9, 2018, DOI 10.1074/jbc.RA118.002913

Aoi Nakazono[‡], Naoko Adachi[‡1], Hideyuki Takahashi[‡2], Takahiro Seki[§], Daizo Hamada[¶‖], Takehiko Ueyama[‡], Norio Sakai[**], and Naoaki Saito[‡3]

From the [‡]Biosignal Research Center, Kobe University, Kobe 657-8501, the [§]Department of Chemico-Pharmacological Sciences, Graduate School of Pharmaceutical Sciences, Kumamoto University, Kumamoto 862-0973 , the [¶]Graduate School of Engineering and [‖]Center for Applied Structural Science (CASS), Kobe University, 7-1-48 Minatojima Minami Machi, Chuo-ku, Kobe 650-0047, and the [**]Department of Molecular and Pharmacological Neuroscience, Graduate School of Biomedical Science, Hiroshima University, Hiroshima 734-8551, Japan

Edited by Ursula Jakob

Amyloid and amyloid-like protein aggregations are hallmarks of multiple, varied neurodegenerative disorders, including Alzheimer's and Parkinson's diseases. We previously reported that spinocerebellar ataxia type 14 (SCA14), a dominant-inherited neurodegenerative disease that affects cerebellar Purkinje cells, is characterized by the intracellular formation of neurotoxic amyloid-like aggregates of genetic variants of protein kinase Cγ (PKCγ). A number of protein chaperones, including heat shock protein 70 (Hsp70), promote the degradation and/or refolding of misfolded proteins and thereby prevent their aggregation. Here, we report that, in various SCA14-associated, aggregating PKCγ variants, endogenous Hsp70 is incorporated into aggregates and that expression of these PKCγ mutants up-regulates Hsp70 expression. We observed that PKCγ binds Hsp70 and that this interaction is enhanced in the SCA14-associated variants, mediated by the kinase domain that is involved in amyloid-like fibril formation as well as the C2 domain of PKCγ. Pharmacological up-regulation of Hsp70 by the Hsp90 inhibitors celastrol and herbimycin A attenuated the aggregation of mutant PKCγ in primary cultured Purkinje cells. Up-regulation of Hsp70 diminished net PKCγ aggregation by preventing aggregate formation, resulting in decreased levels of apoptotic cell death among primary cultured Purkinje cells expressing the PKCγ variant. Of note, herbimycin A also ameliorated abnormal dendritic development. Extending our *in vitro* observations, administration of celastrol to mice up-regulated cerebellar Hsp70. Our findings identify heat shock proteins as important endogenous regulators of pathophysiological PKCγ aggregation and point to Hsp90 inhibition as a potential therapeutic strategy in the treatment of SCA14.

This work was supported by the Joint Research Program of the Biosignal Research Center, Kobe University Grant 281007, and by JSPS KAKENHI Grants JP25293060 and JP17H04032. The authors declare that they have no conflicts of interest with the contents of this article.

This article contains Movie S1.

[1] To whom correspondence may be addressed. Tel.: 81-78-803-5962; Fax: 81-78-803-5971; E-mail: na@gold.kobe-u.ac.jp.

[2] Present address: Cellular Neuroscience, Neurodegeneration and Repair Program, Depts. of Neurology and Neurobiology, Yale University School of Medicine, New Haven, CT 06536.

[3] To whom correspondence may be addressed. Tel.: 81-78-803-5961; Fax: 81-78-803-5971; E-mail: naosaito@kobe-u.ac.jp.

Many neurodegenerative disorders, including Alzheimer's disease, Parkinson's disease, and polyglutamine disease, are characterized by the accumulation of intracellular or extracellular protein aggregates. These aggregates, despite the heterogeneity of their component proteins, typically contain fibrillar amyloid-like structures with common characteristics, such as cross-β-structure and the ability to bind lipophilic dyes such as Congo red (1). Whether fibrillar aggregates are pathogenic, inert, or protective in neurodegenerative diseases still remains controversial. Yet, previous studies have revealed that these aggregates are commonly immunoreactive for molecular chaperones, such as heat shock proteins (Hsps),[4] that facilitate protein folding, assembly, and degradation. Molecular chaperones are potent suppressors of neurodegeneration when overexpressed or induced pharmacologically and therefore represent promising therapeutic targets for amyloid-related neurodegenerative disorders (2).

Autosomal dominant spinocerebellar ataxias (SCAs) are a heterogeneous group of neurodegenerative disorders that are characterized by cerebellar atrophy and progressive ataxia. These disorders can be classified into at least 43 subtypes based on different genetic loci of the causal gene (3). Specifically, SCA14 is caused by a missense mutation or deletion in the *PRKCG* gene, which encodes protein kinase Cγ (PKCγ), a serine/threonine kinase that is highly expressed in the central nervous system and is especially abundant in cerebellar Purkinje cells (PCs) (4–6). More than 30 different PKCγ mutations have been identified in patients with SCA14. Yet, the mechanisms by which mutant PKCγs cause cerebellar atrophy and PC degeneration in SCA14 are unclear. It is known that SCA14-associated mutations increase aggregation of PKCγ in mouse cerebellar PCs *in vivo* and in primary cultured PCs as well as cultured cell lines *in vitro* (7–11). Additionally, PKCγ aggregates form amyloid-like fibrils *in vitro* (12, 13). Thus, it has been

[4] The abbreviations used are: Hsp, heat-shock protein; SCA, spinocerebellar ataxia; PKC, protein kinase C; PC, Purkinje cell; CHO, Chinese hamster ovary; IP, immunoprecipitation; 7-AAD, 7-aminoactinomycin D; HMW, high-molecular weight; DIV, days *in vitro*; 17-DMAG, 17-(dimethylaminoethylamino)-17-demethoxygeldanamycin; HRP, horseradish peroxidase; DMEM, Dulbecco's modified Eagle's medium; a.u., arbitrary unit; pfu, plaque-forming unit; tTA, tetracycline-controlled transactivator; PES-Cl, 2-(3-chlorophenyl)ethynesulfonamide.

hypothesized that the amyloid-like fibril formation of mutant PKCγ is involved in the pathogenesis of SCA14, similar to that of other neurodegenerative disorders.

We recently found that mutant PKCγ up-regulated Hsp70 and that knockdown of endogenous Hsp70 exacerbated mutant PKCγ aggregate formation in primary cultured PCs and cultured neuronal cell lines (14). Given the known role of Hsp70 in neurodegenerative diseases, we hypothesized that Hsp70 might be a therapeutic target against SCA14. In this study, we sought to extend our previous observations by evaluating the effects of Hsp induction in primary cultured PCs expressing mutant PKCγ.

Results

Incorporation and up-regulation of Hsp70 caused by aggregation of mutant PKCγ

To date, 32 point or deletion mutations of PKCγ have been associated with SCA14; of these, 6 and 19 are located in the C1A and C1B diacylglycerol-binding domains, respectively. Additionally, several mutations in the C2 Ca^{2+}-binding domain and kinase domain of PKCγ have been reported (Fig. 1*A*) (12, 15–20). Our previous study showed that Hsp70 (HSPA1A) was incorporated into aggregates of the C1B domain mutants S119P and G128D and that the knockdown of endogenous Hsp70 exacerbated mutant PKCγ-induced cytotoxicity (14). To build on this initial finding, we examined whether the aggregates of various mutants, with mutations located in different domains of PKCγ, were also immunoreactive for Hsp70, using SH-SY5Y cells. This neuroblastoma cell line has been used to study the aggregation of mutant PKCγ in previous studies, and similar results have been obtained in this cell line and in primary cultured Purkinje cells (7, 13, 21). The immunofluorescence analysis showed that all the mutant (R41P, Q127R, V138E, and F643L) PKCγ– green fluorescent proteins (GFPs) tested formed aggregates that co-localized with endogenous Hsp70, whereas most wildtype (WT) PKCγ–GFPs showed diffuse cytoplasmic expression (Fig. 1*B*). Consistent with a previous study (14), the up-regulation of endogenous Hsp70 in cells expressing mutant PKCγs was also observed, and Hsp70 was more highly expressed in cells containing aggregates than in cells without aggregates (Fig. 1*C*). In contrast, Hsc70 (HSPA8), which is a member of the Hsp70 family and is known as a constitutively expressed chaperone, was also incorporated into the PKCγ aggregates, although its endogenous expression levels were not altered by the PKCγ aggregates (Fig. 1*D*). Up-regulation of Hsp70 was evident at 24 h after overexpression of V138E PKCγ–GFP and was significantly enhanced at 48 h (187 ± 44%, compared with 0 h, $n = 4$, $p < 0.01$) in SH-SY5Y cells, although the expression level of Hsc70 was unaffected (Fig. 1*E*). Thus, endogenous Hsp70 chaperones were incorporated into aggregates of various SCA14-associated PKCγ mutants, and Hsp70, but not Hsc70, expression was significantly up-regulated by mutant protein expression.

Interaction of PKCγ with Hsp70 via the C2 and kinase domains is facilitated by a SCA14 mutation

We next tested whether WT and mutant PKCγ physically interact with Hsp70. Co-immunoprecipitation (IP) experiments using COS-7 cells overexpressing FLAG–WT PKCγ, FLAG–V138E PKCγ, and Myc–Hsp70 showed that the Myc–Hsp70 was co-immunoprecipitated with FLAG–WT PKCγ and that the co-IP was significantly enhanced by the SCA14-associated V138E mutation (Fig. 1, *F* and *G*). It is known that Hsp70 preferentially binds to extended polypeptides with exposed hydrophobic residues (22). Interestingly, disorder propensity calculated by IUPred2A (https://iupred2a.elte.hu/) (23, 24), based on the amino acid sequence of PKCγ, indicated a relatively high disorder propensity around C2 and the C terminus of KD compared with C1A and C1B (Fig. 1*H*). These results suggested that C2 and KD may have high tendencies to unfolded for transient periods so that Hsp70 can readily bind to PKCγ through these domains. In fact, co-IP experiments using FLAG-tagged isolated domains (C1A, C1B, C2, and KD) of PKCγ showed that Myc–Hsp70 was significantly co-immunoprecipitated with FLAG-tagged C2 and KD but not FLAG–C1A or -C1B (Fig. 1*I*). These results suggested that PKCγ binds Hsp70 and that the interaction is promoted by a SCA14-associated mutation and mediated by the C2 domain of PKCγ as well as the kinase domain, which is involved in amyloid-like fibril formation (12).

Overexpression of Hsp70 reduces the aggregation of mutant PKCγ

We previously identified WT PKCγ as a novel amyloidogenic protein that forms amyloid-like fibrils, and we found that SCA14-associated mutations accelerated amyloid-like fibril formation in cultured cells (12). Therefore, we next examined whether Hsp70 reduces the aggregation of PKCγ. We assessed CHO and SH-SY5Y cells co-expressing WT or mutant PKCγ–GFPs and Hsp70 or its inactive form (Hsp70–T13G (25, 26)) using fluorescence microscopy, and we counted the numbers of aggregate-containing cells. Overexpression of Hsp70 significantly reduced aggregates of both WT and V138E PKCγ–GFP in CHO (Fig. 2, *A* and *B*) and SH-SY5Y cells (Fig. 2*C*), whereas that of Hsp70–T13G had no significant effects. Although the anti-aggregation effect of Hsp70 was observed in both cell lines, the percentage of SH-SY5Y cells with aggregates was notably lower than that of CHO cells.

To address this issue, we performed an immunoblot analysis and examined the protein expression levels of endogenous Hsps in each cell line. Interestingly, although all the Hsps we tested were expressed in SH-SY5Y cells, the immunoreactive bands of Hsp70 and Hsp27 were below the detectable levels in CHO cells under basal conditions (Fig. 2, *D* and *E*). Moreover, Hsp70 up-regulation by overexpression of V138E PKCγ–GFP was not observed in CHO cells (Fig. 2*F*). Thus, it is plausible that the aggregation levels of mutant PKCγ–GFP are inversely associated with the expression level of endogenous Hsps. We next examined the dominant-negative effect of Hsp70 using Hsp70–K71E, which exhibits intact substrate association, but weakens ATP binding (27), on aggregate formation in SH-SY5Y cells. Consistent with the results from a previous study that included knockdown experiments (14), Hsp70–K71E significantly exacerbated the aggregation of various mutants, but not WT PKCγ–GFP, in SH-SY5Y cells (Fig. 2*G*). Together, these results strongly suggested that Hsp70 is critical for preventing the aggregation of mutant PKCγ.

Overexpression of Hsp70 ameliorates mutant PKCγ cytotoxicity

We previously showed that mutant PKCγ overexpression induces cell death (9). Therefore, in this study, we examined whether Hsp70 overexpression could suppress mutant PKCγ-induced cell death in CHO cells. To achieve this, CHO cells overexpressing both WT or mutant PKCγ–GFP and Hsp70 were assessed after transfection for 48 h. Because the dead cells

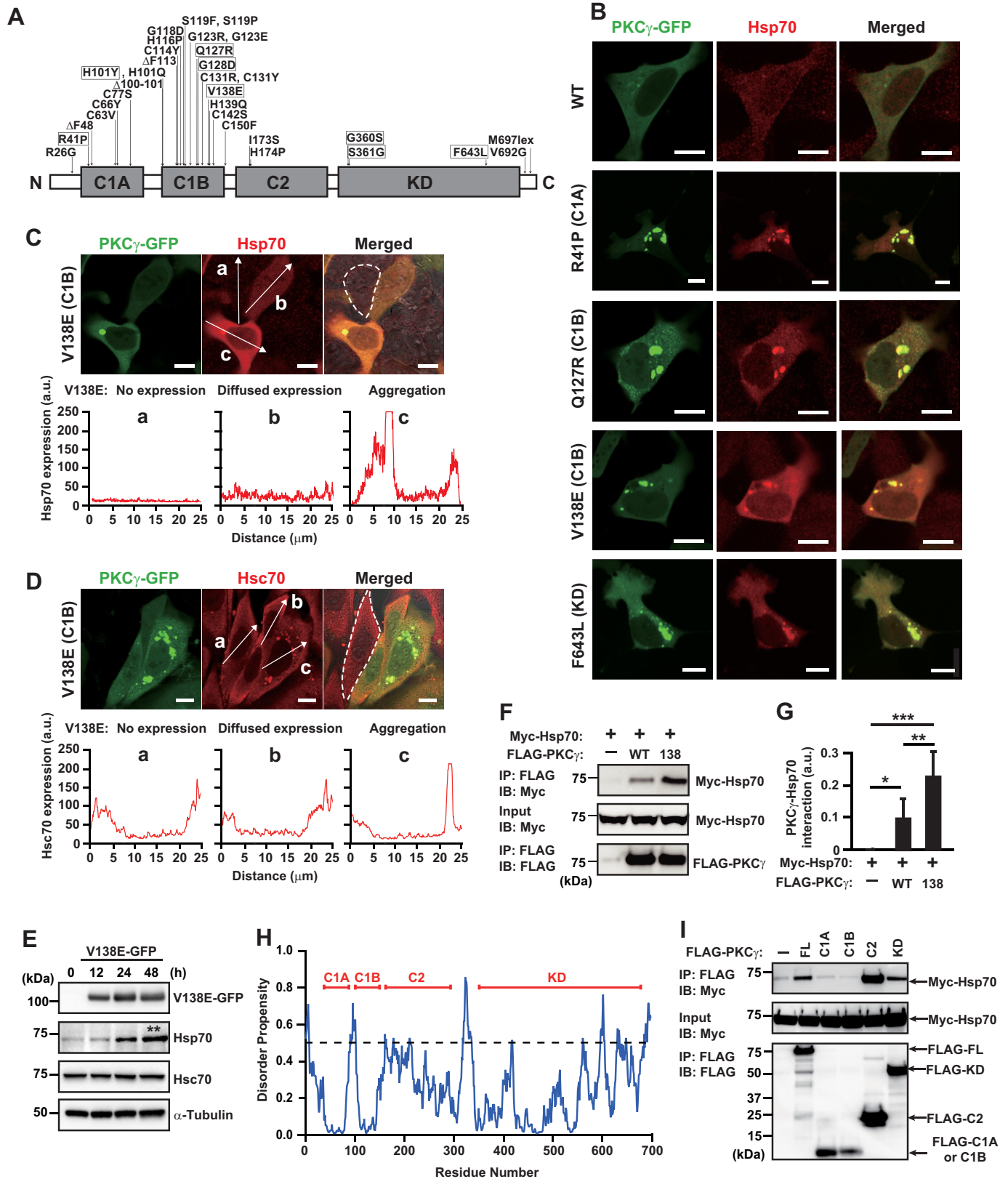

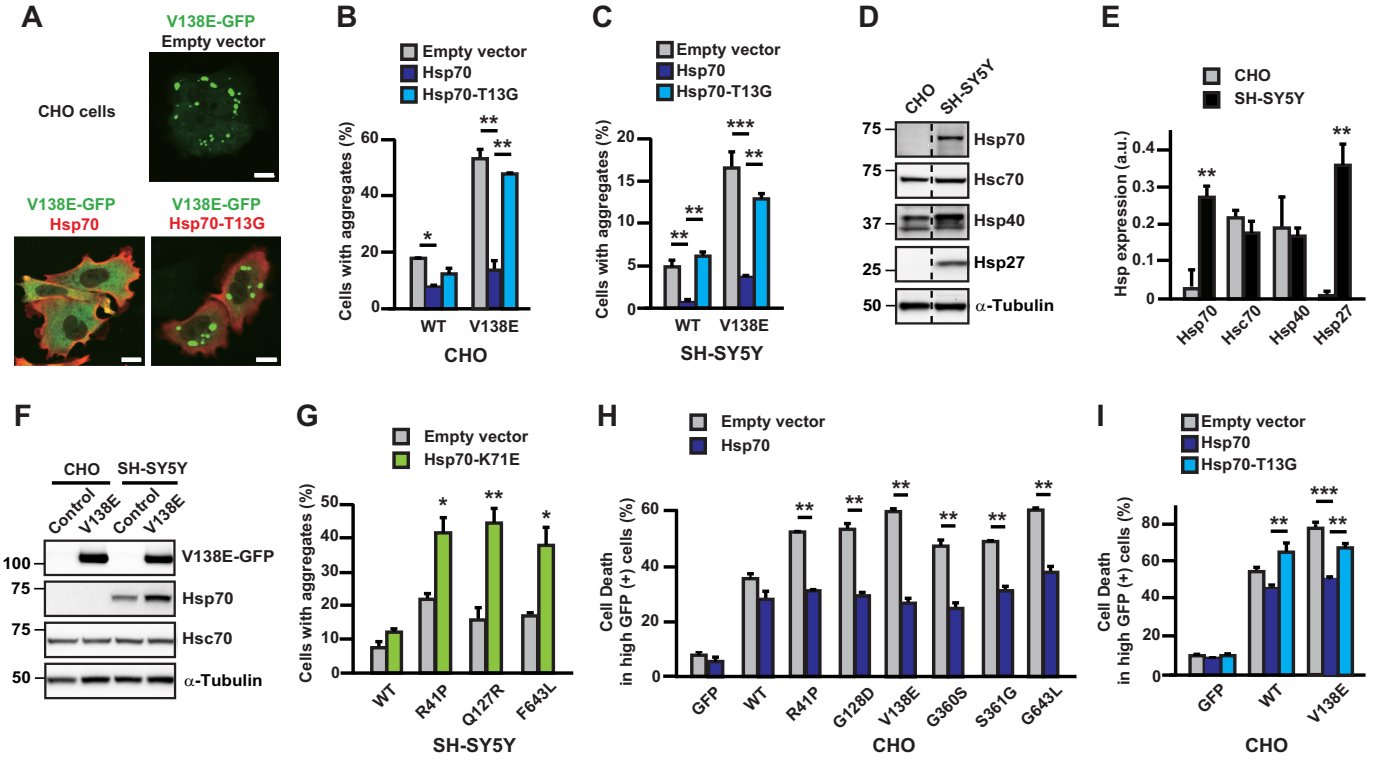

Figure 2. Overexpression of Hsp70 reduces the aggregation and cell death induced by mutant PKCγ. *A*, representative images of cells expressing V138E PKCγ–GFP (*green*) and empty vector, Hsp70 (*red*), or Hsp70–T13G (*red*) in CHO cells. *Scale bar* = 10 μm. *B* and *C*, CHO (*B*) and SH-SY5Y (*C*) cells expressing WT or V138E PKCγ–GFP and Hsp70 or Hsp70–T13G were quantified to obtain the percentage of cells containing aggregates. One to 2 days after transfection, the cells were fixed, permeabilized, and incubated with anti-Hsp70 antibody. At least 300 GFP- and Hsp70-positive cells were counted. Mean ± S.E. of the mean, $n = 2$–3. *, $p < 0.05$; **, $p < 0.01$; and ***, $p < 0.001$; one-way analysis of variance with Tukey's post hoc tests. *D*, representative immunoblots with anti-Hsp70, Hsc70, Hsp40, Hsp27, and α-tubulin antibodies using CHO and SH-SY5Y cell lysates. *E*, quantification of the results shown in *D*. $n = 4$. **, $p < 0.01$; one-way analysis of variance with Tukey's post hoc tests. *F*, representative immunoblots with anti-PKCγ, Hsp70, Hsc70, and α-tubulin antibodies using CHO and SH-SY5Y cell lysates with or without V138E PKCγ–GFP expression. The cells were assessed 1 day after transfection. *G*, SH-SY5Y cells expressing WT, R41P, Q127R, or F643L PKCγ–GFP and Hsp70–K71E were quantified to obtain the percentage of cells containing aggregates. One day after transfection, the cells were fixed, permeabilized, and incubated with anti-Hsp70 antibody. At least 200 GFP- and Hsp70-positive cells were counted. Mean ± S.E. of the mean, $n = 3$. *, $p < 0.05$, and **, $p < 0.01$; Student's *t* test. *H*, percentages of cell death in high GFP-positive cells. Two days after transfection, the CHO cells were harvested and assessed by flow cytometry. Mean ± S.E. of the mean, $n = 3$. *, $p < 0.05$, and **, $p < 0.01$; Student's *t* test. *I*, mean percentages of cell death in high GFP-positive cells. Two days after transfection, the CHO cells were harvested and assessed by flow cytometry. Mean ± S.E. of the mean, $n = 3$. *, $p < 0.05$; **, $p < 0.01$; and ***, $p < 0.001$; one-way analysis of variance with Tukey's post hoc tests.

were detached from the cultured dishes (12), floating cells in the medium as well as attached cells on the dishes were harvested for the analysis. The cells were stained with 7-aminoactinomycin D (7-AAD), a fluorescent DNA dye that selectively stains the DNA of dead cells (28). Stained cells were assessed using flow cytometry and classified in accordance with GFP and 7-AAD fluorescence. Because mutant PKCγ–GFP-induced cell death has been observed in parallel with its expression level (9), cells with relatively high GFP fluorescence were extracted to examine the effect of Hsp70 overexpression. Cells expressing Hsp70 exhibited significant reduction in cell death caused by various mutant PKCγ–GFPs (Fig. 2*H*), whereas the co-expression of Hsp70–T13G, an inactive form of Hsp70, had no effect on mutant PKCγ cytotoxicity (Fig. 2*I*), suggesting that the chaperon activity of Hsp70 is required to protect against cell death caused by SCA14-associated mutants. Taken together, we found that inhibition of PKCγ aggregation by Hsp70 ameliorated mutant PKCγ-induced cell death in CHO cells.

Figure 1. Hsp70 (HSPA1A) physically interacts with PKCγ via the C2 and kinase domains. *A*, locations of representative mutations associated with SCA14 and domains of PKCγ. Mutants assessed in this study are indicated in *boxes*. *B*, representative confocal images of co-localization of endogenous Hsp70 (*red*) with the aggregates of R41P, Q127R, V138E, and F643L PKCγ–GFP (*green*) in SH-SY5Y cells; C1A, C1B, and KD, in *parentheses*, indicate the domain locations of each mutation. One day after transfection, the cells were fixed, permeabilized, and incubated with anti-Hsp70 antibody. *Scale bar* = 10 μm. *C* and *D*, representative Hsp70 (*C*) and Hsc70 (*D*) immunofluorescence images of SH-SY5Y cells with no overexpression (*panel a*), diffuse expression (*panel b*), and V138E PKCγ–GFP aggregation (*panel c*). One day after transfection, the cells were fixed, permeabilized, and incubated with anti-Hsp70 (*C*) and anti-Hsc70 (*D*) antibodies. A cell without overexpression of V138E PKCγ–GFP has been marked by a *dashed line*. The fluorescence intensity of Hsp70 and Hsc70, measured along the *arrows* (*panels a–c*), is shown in the *bottom panels*. *Scale bar* = 10 μm. *E*, representative immunoblots with anti-PKCγ, Hsp70, Hsc70, and α-tubulin antibodies using SH-SY5Y cell lysates expressing V138E PKCγ–GFP for the indicated times after transfection. Four independent experiments were performed, and the Hsp70 or Hsc70 band intensities of all conditions are normalized against α-tubulin. *, $p < 0.05$; **, $p < 0.01$ (0 h *versus* 48 h); one-way analysis of variance with Tukey's post hoc tests. *F*, co-immunoprecipitation (*IP*) of FLAG–PKCγ and Myc–Hsp70 was detected by immunoblotting (*IB*) in COS-7 cells. The cells were harvested and assessed 1 day after transfection. *G*, quantification of the results shown in *F*. Intensity of the immunoprecipitated bands of Myc–Hsp70 was normalized by their input. Mean ± S.D, $n = 7$. *, $p < 0.05$; **, $p < 0.01$; and ***, $p < 0.001$; one-way analysis of variance with Tukey's post hoc tests. *H*, intrinsic disorder propensity of the amino acid sequence of PKCγ calculated by IUPred2A (https://iupred2a.elte.hu/). *I*, co-immunoprecipitation of the FLAG-tagged full-length (*FL*) C1A, C1B, C2, or KD of PKCγ and Myc–Hsp70 in COS7 cells. The cells were harvested and assessed 1 day after transfection. Similar results were obtained in at least three independent experiments. *SCA14* = spinocerebellar ataxia type 14.

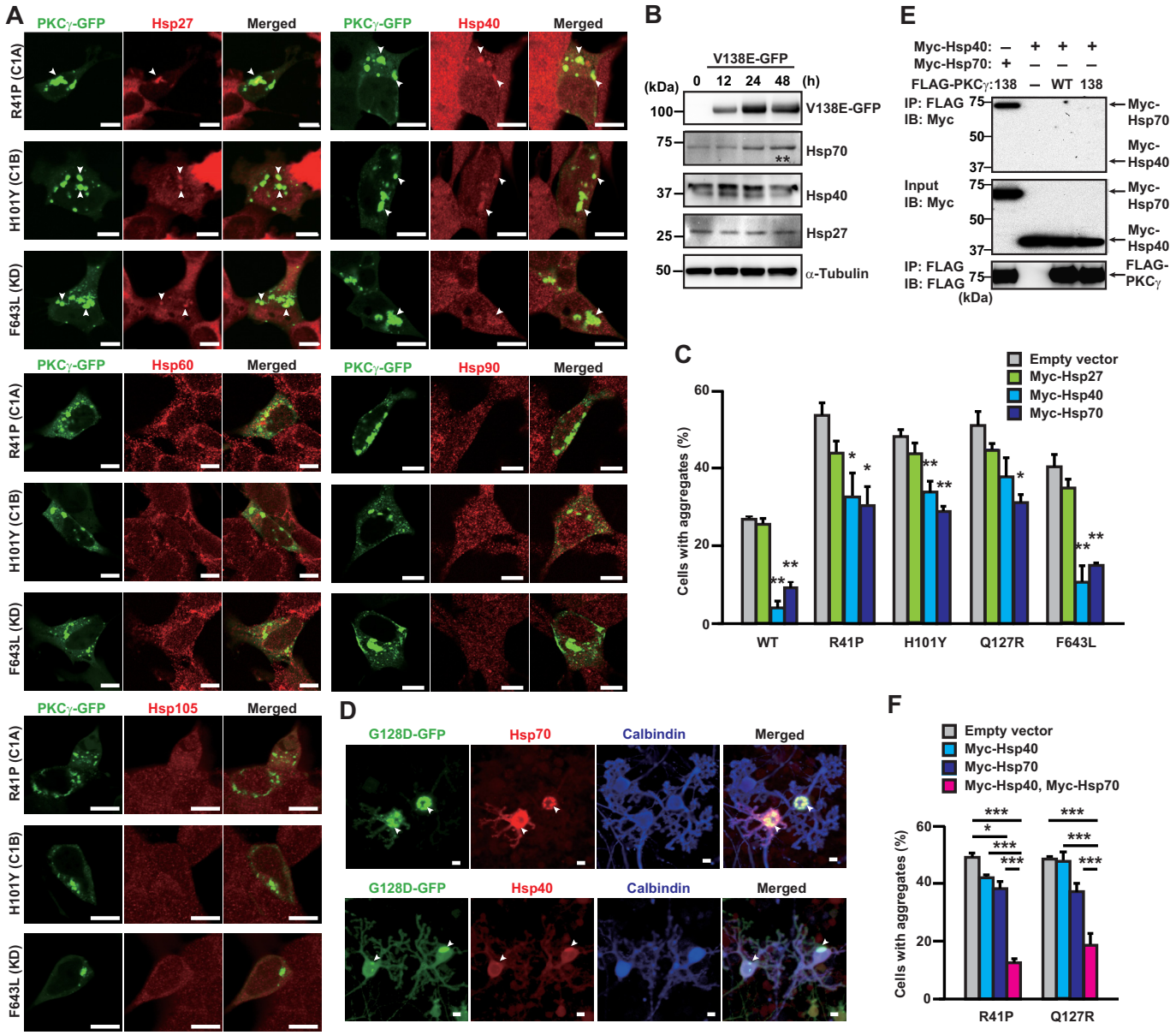

Figure 3. Co-expression of Hsp70 and Hsp40 synergistically suppresses PKCγ aggregation. *A*, representative confocal images of the localization of endogenous Hsps (*red*) with the aggregates of R41P, H101Y, and F643L PKCγ–GFP (*green*) in SH-SY5Y cells; C1A, C1B, and KD, in *parentheses*, indicate the domain locations of each mutation. One day after transfection, the cells were fixed, permeabilized, and incubated with antibodies against Hsps. *Arrowheads* indicate co-localized PKCγ–GFP and Hsps. *Scale bar* = 10 μm. *B*, representative immunoblots with anti-PKCγ, Hsp70, Hsp40, Hsp27, and α-tubulin antibodies using SH-SY5Y cell lysate expressing V138E PKCγ–GFP. Four independent experiments were performed, and the Hsp70, Hsp40, or Hsp27 band intensities for all conditions are normalized against α-tubulin. **, $p < 0.01$ (0 h *versus* 48 h); one-way analysis of variance with Tukey's post hoc tests. *C*, CHO cells expressing WT, R41P, H101Y, Q127R, or F643L PKCγ–GFP, and Myc–Hsp27, Myc–Hsp40, and/or Myc–Hsp70 were quantified to obtain the percentage of cells containing aggregates. Two days after transfection, the cells were fixed, permeabilized, and incubated with anti-Myc antibody. At least 200 GFP- and Myc-positive cells were counted. Mean ± S.E. of the mean, $n = 3$. *, $p < 0.05$, and ***, $p < 0.001$; one-way analysis of variance with Tukey's post hoc tests. *D*, representative confocal images of the localization of endogenous Hsps (*red*) with aggregates of G128D PKCγ–GFP (G128D–GFP, *green*) in primary cultured PCs. On DIV 21, PC-specific expression of G128D–GFP was achieved with adenoviral infection of Ad-L7–tTA. After 5 days of incubation, the PCs were fixed, permeabilized, and incubated with antibodies against Hsps. Calbindin (*blue*) was a marker for Purkinje cells. *Arrowheads* indicate co-localized G128D–GFP and Hsps. *Scale bar* = 10 μm. *E*, co-immunoprecipitation of WT or V138E FLAG–PKCγ with Myc–Hsp40; no co-immunoprecipitation was observed in COS-7 cells. One day after transfection, the cells were harvested and assessed. *F*, CHO cells expressing R41P or Q127R PKCγ–GFP and Myc–Hsp40 and/or Myc–Hsp70 were quantified to obtain the percentage of cells containing aggregates. Two day after transfection, the cells were fixed, permeabilized, and incubated with anti-Myc antibodies. At least 200 GFP- and Myc-positive cells were counted. Mean ± S.E. of the mean, $n = 3$. *, $p < 0.05$, and ***, $p < 0.001$; one-way analysis of variance with Tukey's post hoc tests.

Hsp70 and Hsp40 synergistically reduce aggregation of mutant PKCγ

We next explored the effects of other molecular chaperons on mutant PKCγ aggregation in SH-SY5Y cells. Immunocytochemical analyses revealed that endogenous Hsp27 (HSPB1) and Hsp40 (DNAJB1), but not Hsp60 (HSPD1), Hsp90 (HSP90AA/HSP90AB), or Hsp105 (HSPH1), were incorporated into mutant PKCγ–GFP aggregates (Fig. 3*A*). Endogenous expression levels of Hsp27 and Hsp40, but not of Hsp70, in SH-SY5Y cells were not altered by overexpression of V138E

PKCγ–GFP (Fig. 3*B*). To verify the effects of incorporated Hsps, Myc–Hsp27, Myc–Hsp40, or Myc–Hsp70 was co-expressed with various mutant PKCγ–GFPs in CHO cells, and percentages of cells containing aggregates were counted. Similar to Hsp70, overexpression of Hsp40 reduced the aggregation of several mutant PKCγ–GFPs (Fig. 3*C*). Conversely, Hsp27 had no effect. Therefore, we confirmed the incorporation of endogenous Hsp70 and Hsp40 into PKCγ aggregates using primary cultured PCs. The PC-specific expression of G128D PKCγ–GFP (G128D–GFP) was achieved with adenoviral infection of Ad-L7–tTA (tetracycline-controlled transactivator), which expresses tTA in a PC-specific manner, and Ad-TetOP–PKCγ–GFP on days *in vitro* 21 (DIV 21) (29); G128D is a C1B domain mutant that forms aggregates with high frequency (9). As shown in Fig. 3*D*, both Hsp70 and Hsp40 were incorporated into the aggregates in calbindin-positive PCs. Although Myc–Hsp40 did not show direct interaction with FLAG–PKCγ in a co-IP assay (Fig. 3*E*), Hsp40 is known as a co-chaperone of Hsp70, and the interaction between Hsp40 and Hsp70 has been previously reported (30). Therefore, Hsp40 may have indirectly interacted with PKCγ aggregates through Hsp70. We next examined whether Hsp70 and Hsp40 exhibit synergistic effects on the aggregation. As shown in Fig. 3*F*, the co-expression of Myc–Hsp40 and Myc–Hsp70 in CHO cells produced a dramatic suppression of mutant PKCγ aggregation. Among Hsps, both Hsp70 and Hsp40 are key components for diminishing aggregation of mutant PKCγ.

Overexpression or pharmacological induction of Hsps increases the detergent solubility of mutant PKCγ

It has been reported that detergent-insoluble mutated proteins are generated in the cellular and animal models of various neurodegenerative diseases (31–33). We have also shown that SCA14-associated mutations in PKCγ increase its insolubility in Triton X-100, a nonionic detergent (9). Thus, we next examined whether Hsps affect the detergent solubility of mutant PKCγ. Transfected CHO cells were separated into 1% Triton X-100–soluble and -insoluble fractions, and both fractions were separated using SDS-PAGE under nonreducing conditions. Western blot analysis revealed the presence of high-molecular weight (HMW) species (>150 kDa) as well as SDS-soluble monomeric FLAG–Q127R PKCγ in the Triton X-100–insoluble fraction (Fig. 4*A*), suggesting amyloid-like fibril formation by mutant PKCγ, as reported previously (12). The amounts of whole-monomeric and HMW FLAG–Q127R PKCγ in both fractions were quantified by immunoblotting with anti-FLAG antibody, and the percentage distributions of monomeric and HMW PKCγ in the Triton X-100–soluble and -insoluble fractions were determined (Fig. 4, *B* and *C*). Overexpression of Myc–Hsp70 or Myc–Hsp40 alone significantly reduced HMW PKCγ immunoreactivity in the Triton X-100–insoluble fraction. Moreover, co-expression of Myc–Hsp70 and Myc–Hsp40 dramatically reduced HMW PKCγ in the Triton X-100–insoluble fraction and increased monomeric and HMW PKCγ in the Triton X-100–soluble fraction, consistent with the results shown in Fig. 3*E*. These results indicated that co-expression of Hsp40 and Hsp70 synergistically improved the detergent solubility of mutant PKCγ and reduced its aggregation.

Celastrol, a member of the triterpenoid compound family, extracted from the root of *Tripterygium wilfordii* Hook F (Thunder of God Vine), is a known Hsp90 inhibitor that activates heat shock transcription factor 1 (HSF1), a major transcription factor for Hsps (34, 35). It has been reported that celastrol treatment induces Hsps and reduces aggregation and cell toxicity in a cell culture model of polyglutamine disease (36). Therefore, we asked whether the up-regulation of Hsps by celastrol could alleviate mutant PKCγ aggregation in SH-SY5Y cells. Celastrol treatment (3 μM, 3 h) up-regulated endogenous Hsp70 and Hsp40 expression and reduced monomeric and HMW PKCγ in the Triton X-100–insoluble fraction of Q127R PKCγ–GFP compared with dimethyl sulfoxide (DMSO) treatment (Fig. 4, *D–G*). These results indicated that Hsp70 and Hsp40 up-regulation by celastrol alleviated the aggregation of mutant PKCγ *in vitro*.

Hsp90 inhibition induces Hsp70 expression in PCs in vitro, and celastrol up-regulates Hsp70 in the mouse cerebellum in vivo

Although previous studies have shown that treatment with celastrol and herbimycin A, a benzoquinone ansamycin inhibitor of Hsp90, induces Hsp expression in various *in vitro* and *in vivo* models (36–38), it is not known whether the treatment also induces Hsps in PCs of the mouse cerebellum. Thus, we examined the effect of celastrol and herbimycin A treatment on Hsp expression in PCs *in vitro*. Immunoblot analyses showed that both celastrol (3 μM for 1 h, after which the cells were cultured for 23 h without celastrol) and herbimycin A (2 μM for 24 h) treatments successfully up-regulated Hsp70 in primary cultured cerebellar cells (Fig. 5, *A* and *B*). In contrast to the results from SH-SY5Y cells (Fig. 4, *D* and *E*), Hsp40 expression was not up-regulated by Hsp90 inhibitors. Moreover, Hsc70 expression was not altered by Hsp90 inhibitors. To confirm the up-regulation of Hsp70 in PCs, celastrol-treated (3 μM, 1 h/day, for 4 days) or herbimycin A-treated (2 μM for 4 days) PCs were assessed using fluorescence microscopy. Both Hsp90 inhibitors enhanced Hsp70 expression in calbindin-positive PCs (Fig. 5*C*). We next tested the brain permeability of intraperitoneally administered celastrol and herbimycin A in C57BL/6N mice. Notably, Hsp70, but not Hsp40, was up-regulated in cerebellar lysates by celastrol treatment (1 mg/kg) (Fig. 5*D*), although herbimycin A (2 mg/kg) had no effect on Hsp expression at 2 weeks (Fig. 5*E*). These results indicate that Hsp90 inhibition by celastrol or herbimycin A induced Hsp70 expression in PCs *in vitro*, and celastrol penetrated the mouse cerebellum and up-regulated Hsp70 *in vivo*.

Pharmacological Hsp70 induction inhibits aggregation in PCs expressing mutant PKCγ

We investigated the ability of celastrol or herbimycin A treatment to diminish mutant PKCγ aggregation in PCs. The PC-specific expression of G128D–GFP was achieved with adenoviral infection on DIV 21. Drug treatments were started on DIV 26 when most PCs expressing mutant PKCγs already contained

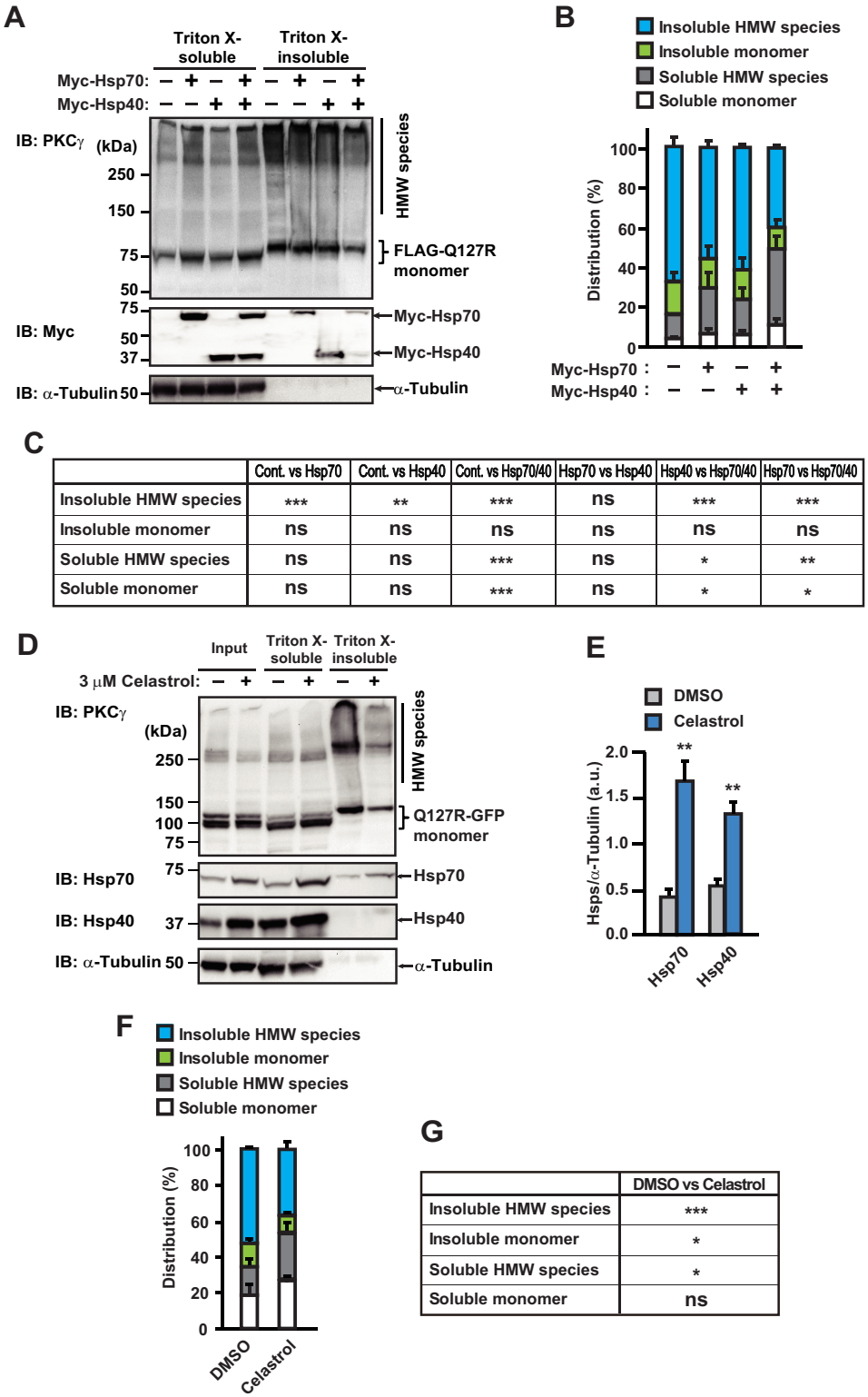

	Cont. vs Hsp70	Cont. vs Hsp40	Cont. vs Hsp70/40	Hsp70 vs Hsp40	Hsp40 vs Hsp70/40	Hsp70 vs Hsp70/40
Insoluble HMW species	***	**	***	ns	***	***
Insoluble monomer	ns	ns	ns	ns	ns	ns
Soluble HMW species	ns	ns	***	ns	*	**
Soluble monomer	ns	ns	***	ns	*	*

	DMSO vs Celastrol
Insoluble HMW species	***
Insoluble monomer	*
Soluble HMW species	*
Soluble monomer	ns

Figure 4. Triton X-100 insolubility of mutant PKCγ–GFP is decreased by the overexpression or pharmacological induction of Hsps. *A*, representative blots of the Triton X-100–soluble and -insoluble fractions of CHO cells overexpressing FLAG–Q127R PKCγ and Myc–Hsps. *B*, quantification of the percentage distribution of monomer and HMW species of FLAG–Q127R PKCγ in the Triton X-100–soluble and -insoluble fractions in *A*. Mean ± S.D., $n = 4$. *C*, statistical table for *B*. *, $p < 0.05$; **, $p < 0.01$; and ***, $p < 0.001$; one-way analysis of variance with Tukey's post hoc tests; *ns* indicates not significant. *D*, representative blots of the Triton X-100–soluble and -insoluble fractions of the SH-SY5Y cells overexpressing Q127R PKCγ–GFP treated with celastrol (3 μM for 3 h) or DMSO. *E*, quantification of Hsp70 and Hsp40 expression induced by celastrol. Mean ± S.D., $n = 3$. **, $p < 0.01$; Student's *t* test. *F*, quantification of the percentage distribution of monomer and HMW species of Q127R PKCγ–GFP in the Triton X-100–soluble and -insoluble fractions. Mean ± S.D., $n = 3$. *G*, statistical table for *F*. *, $p < 0.05$, and ***, $p < 0.001$; Student's *t* test; *ns* indicates not significant.

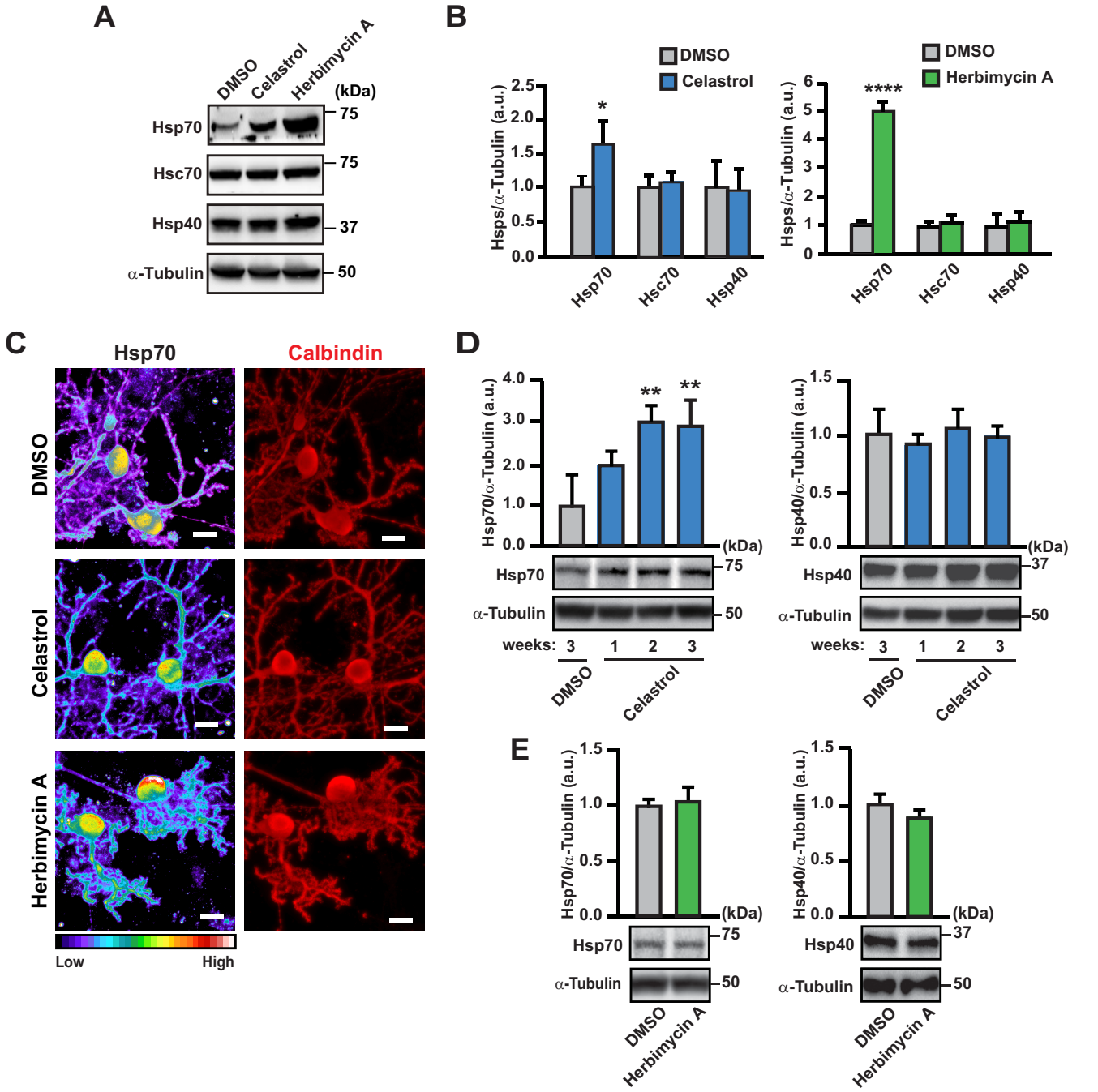

Figure 5. Hsp90 inhibition induces Hsp70 expression in primary cultured PCs and the mouse cerebellum. *A*, representative immunoblots with anti-Hsp70, Hsc70, Hsp40, and α-tubulin antibodies using primary cerebellar cell lysate treated with Hsp90 inhibitors. The cells were treated with celastrol (3 μM for 1 h, followed by incubation for 23 h), herbimycin A (2 μM, 24 h), or DMSO. *B*, quantification of endogenous Hsp70, Hsc70, and Hsp40 expression levels in *A*. Mean ± S.D., $n = 4$. *, $p < 0.05$, and ****, $p < 0.0001$; one-way analysis of variance with Tukey's post hoc tests. *C*, representative confocal images of primary cultured PCs treated with celastrol (3 μM, 1 h/day, for 4 days) or herbimycin A (2 μM, 24 h, for 4 days) and stained with anti-Hsp70 and calbindin antibodies. The Hsp70 fluorescence intensity is converted to pseudo-color to show the expression levels. *Scale bar* = 10 μm. *D*, mice were treated with intraperitoneal (i.p.) celastrol (1 mg/kg) or DMSO daily for 1, 2, or 3 weeks. Immunoblot analysis showed that celastrol treatment induced endogenous Hsp70 (*left*), but not Hsp40 (*right*), in the cerebellum. Mean ± S.D., $n = 4$. **, $p < 0.01$; one-way analysis of variance with Tukey's post hoc tests. *E*, mice were treated with herbimycin A (2 mg/kg, i.p.) or DMSO daily for 2 weeks. Mean ± S.D., $n = 3$. Student's *t* test.

aggregates. After treatment with celastrol (3 μM, 1 h/d) or herbimycin A (2 μM, 24 h) for 4 days, PCs were fixed and stained with antibody against calbindin and assessed using fluorescence microscopy (Fig. 6*A*). To assess the intensity of aggregates, GFP fluorescence was converted into rainbow pseudocolor. As shown in Fig. 6*B*, aggregates were dispersed, and the intensities were lowered after the Hsp90 inhibitor treatments. To quantify the effects of drug treatment on aggregate formation, the numbers of cells containing high-intensity aggregates, which appear as white spots (intensity exceeding 250 arbitrary units (a.u.)) in calbindin-positive PCs, were counted, and the percentages of cells containing high-intensity aggregates were calculated. Both celastrol and herbimycin A treatments significantly diminished the high-intensity aggregates in PCs (Fig. 6*C*).

Because celastrol is known to induce autophagy (39, 40), we examined whether Hsp90 inhibitors induce activation of autophagy to enhance the aggregate clearance in primary cultured cerebellar cells. Autophagic activation was assessed by the level of LC3-II, a membrane-bound form of LC3 as a marker of autophagic activity (41). As a positive control for LC3-II detection, chloroquine, which is an autophagy inhibitor, was used to accumulate LC3-II. In agreement with previous reports, immunoblot analysis showed that chloroquine as well as celastrol significantly increases LC3-II levels, whereas herbimycin A has no effect (Fig. 6*D*). Thus, although in the case of celastrol the autophagic activation may also contribute to the clearance of the PKCγ aggregates, herbimycin A treatment does not appear to induce autophagy in primary cultured cerebellar cells.

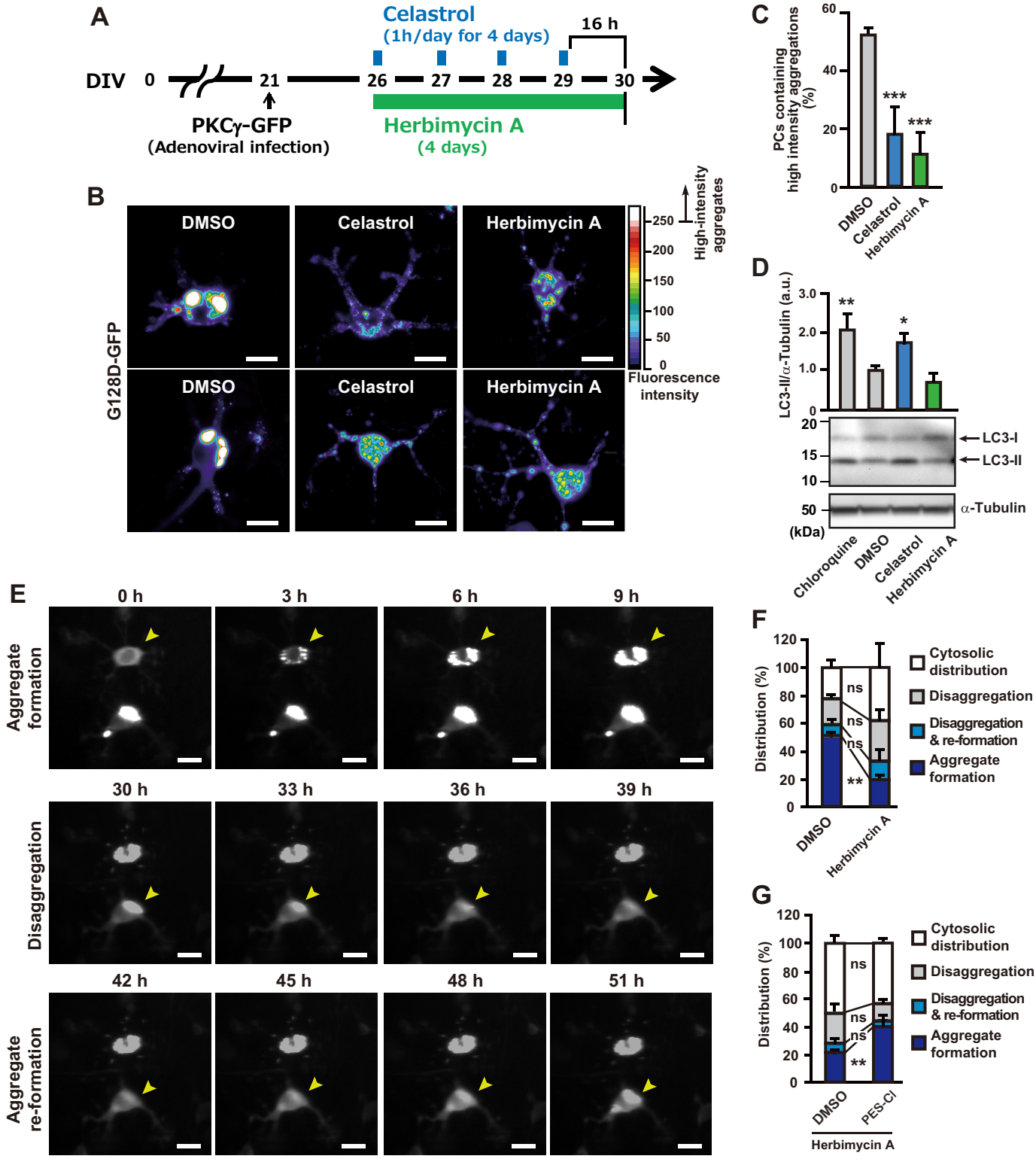

Aggregation of mutant PKCγ is a dynamic process regulated by Hsp70

To examine in more detail the diminishment of aggregated PKCγ by pharmacological enhancement of Hsp70 expression, we performed long-term time-lapse imaging of primary cerebellar cultures in which G128D–GFP was overexpressed by adenoviral infection under the PC-specific L7 promoter. GFP fluorescence was assessed hourly for 51 h, beginning 5 days after infection. We imaged 7–10 fields in each of the cultures, which were treated with either DMSO alone (vehicle control) or herbimycin A. Herbimycin A treatment was used to avoid the induction of autophagic activity. Remarkably, we observed dynamic formation and dissolution of aggregates. In control cultures, over the course of observation, aggregates were observed in 78.1% of the cells, including cells in which aggregates formed (51.2%), and in which aggregates formed and disassembled (19.0%) or formed, disassembled, and re-formed (7.9%); aggregates were lost in some cells that initially included aggregates (*i.e.* at time 0 h), and aggregation in these cells could be restored over time (Fig. 6, *E* and *F* and supporting Movie S1). Thus, there is a dynamic equilibrium between disaggregated and aggregated mutant PKCγ, which may reflect, under these conditions, an influence of endogenous WT Hsp. In cultures treated with herbimycin A, the number of cells containing aggregates over the time course of 51 h was diminished (61.9% *versus* 78.1%; not significant), which included cells in which aggregates formed (19.0% *versus* 51.2%; significant) and in which aggregates formed and disassembled (28.9% *versus* 19%; not significant), and formed, disassembled, and re-formed (14.0% *versus* 7.9%, not significant), indicating that the induction of Hsp70 prevents the formation of aggregates (Fig. 6*F*). These results are consistent with the end-point measurements presented in Fig. 6, *B* and *C*.

To further demonstrate a role of Hsp70 in the dynamic process of aggregation, we examined the effect of a cell-permeable Hsp70 inhibitor, PES-Cl, on herbimycin A-treated PCs. In detail, to induce endogenous Hsp70 expression, PCs were treated with herbimycin A for 8 h before addition of PES-Cl (2 μM) or DMSO. GFP fluorescence was then assessed hourly for 46 h. In cultures treated with herbimycin A and PES-Cl, the number of cells that formed aggregates was significantly enhanced (Fig. 6*G*). Thus, drug-induced up-regulation of Hsp70 is able to shift the dynamic equilibrium governing amyloid formation toward the cytosolic form of PKCγ.

Herbimycin A attenuates the impairment of dendritic development and inhibits apoptosis in PCs expressing mutant PKCγ–GFP

We investigated the ability of celastrol or herbimycin A treatment to ameliorate dysfunction induced by mutant PKCγ expression in PCs. Consistent with a previous study, WT PKCγ–GFP exhibited ubiquitous GFP fluorescence in the cytoplasm and dendrites, whereas G128D–GFP formed aggregates in the soma and was associated with abnormal dendritic development (Fig. 7*A*) (7). We next examined dendritic development, as assessed by dendritic length, number of nodes, and number of terminals, in PCs. Herbimycin A treatment significantly improved the abnormal dendritic development induced by G128D–GFP in PCs but had no effect on dendritic parameters in PCs expressing WT PKCγ–GFP (Fig. 7, *B–E*). In contrast, celastrol treatment failed to improve dendritic development in PCs expressing G128D–GFP and elicited dendritic regression in PCs expressing WT PKCγ–GFP.

Finally, we investigated the effect of celastrol and herbimycin A treatments on PC apoptosis induced by mutant PKCγ–GFP expression. Apoptosis was assessed by chromatin condensation or fragmentation in calbindin-positive PCs (Fig. 7*F*) (7, 13). The ratio of apoptotic PCs expressing G128D–GFP was significantly higher than that of PCs expressing WT PKCγ–GFP (Fig. 7*G*). Additionally, both celastrol and herbimycin A treatments significantly reduced the number of apoptotic PCs expressing G128D–GFP but had no effects on the PCs expressing WT PKCγ–GFP (Fig. 7*G*). Taken together, both celastrol and herbimycin A induced Hsp70 expression and diminished the aggregation of mutant PKCγ, which ameliorated the apoptosis induced by mutant PKCγ in primary cultured PCs. Furthermore, herbimycin A restored abnormal dendritic development in these PCs.

Discussion

In this study, we examined strategies for alleviating the neurotoxic effects of mutant PKCγ aggregation in an *in vitro* model of SCA14, and we found that pharmacological induction of Hsp70 ameliorated mutant PKCγ toxicity. The induction of Hsp70 by the Hsp90 inhibitors celastrol and herbimycin A inhibited mutant PKCγ aggregation and reduced apoptosis in PCs. Herbimycin A also improved abnormal dendrite development in PCs. Celastrol, but not herbimycin A, induced Hsp70 expression in the mouse cerebellum *in vivo* and thus represents a potential therapeutic strategy against SCA14.

Figure 6. Pharmacological induction of Hsp70s reduce mutant PKCγ aggregation in primary cultured PCs. *A,* scheme of the pharmacological treatments of primary cultured PCs. The PC-specific expression of PKCγ–GFP was achieved with adenoviral transduction on DIV 21. Celastrol (3 μM, 1 h/day, for 4 days) or herbimycin A (2 μM for 4 days) was started on DIV 26. After a 4-day treatment period, PCs were fixed and stained for calbindin and assessed using fluorescence microscopy. *B*, representative confocal images of PCs expressing G128D–GFP with GFP fluorescence intensity converted to pseudo-color. *White spots* indicate high-intensity aggregates of PKCγ–GFP. The *upper* and *lower panels* show results from two separate fields of view. *Scale bar* = 10 μm. *C*, percentage of PCs containing high-intensity aggregates of G128D–GFP in *B*. Mean ± S.D., $n = 3$. ***, $p < 0.001$; one-way analysis of variance with Tukey's post hoc tests. *D*, representative immunoblots with anti-LC3 and α-tubulin antibodies using primary cerebellar cell lysates treated with chloroquine (50 μM for 17 h), DMSO, celastrol (3 μM for 1 h, followed by incubation for 23 h), or herbimycin A (2 μM, 24 h). Three independent experiments were performed, and the LC3-II band intensities of all conditions are normalized by α-tubulin. Mean ± S.D., *, $p < 0.05$; **, $p < 0.01$; one-way analysis of variance with Tukey's post hoc tests. *E*, representative images of PCs expressing G128D–GFP evaluated by long-term time-lapse imaging. Images were captured every 1 h for 51 h, and the data were analyzed using MetaMorph software. The representative videos are available in Movie S1. *Scale bar* = 10 μm. $n = 3$. *F* and *G*, percentage of PCs that showed aggregate formation, disaggregation, disaggregation/re-formation, or cytosolic distribution of G128D–GFP. The cells were observed for 51 h with DMSO or herbimycin A (2 μM) treatment (*F*). *G*, after 8 h of 2 μM herbimycin A treatment, DMSO or PES-Cl (10 μM) was added to the medium, and the cells were observed for 46 h. Mean ± S.D., $n = 3$. **, $p < 0.01$; Student's *t* test. *ns* indicates not significant.

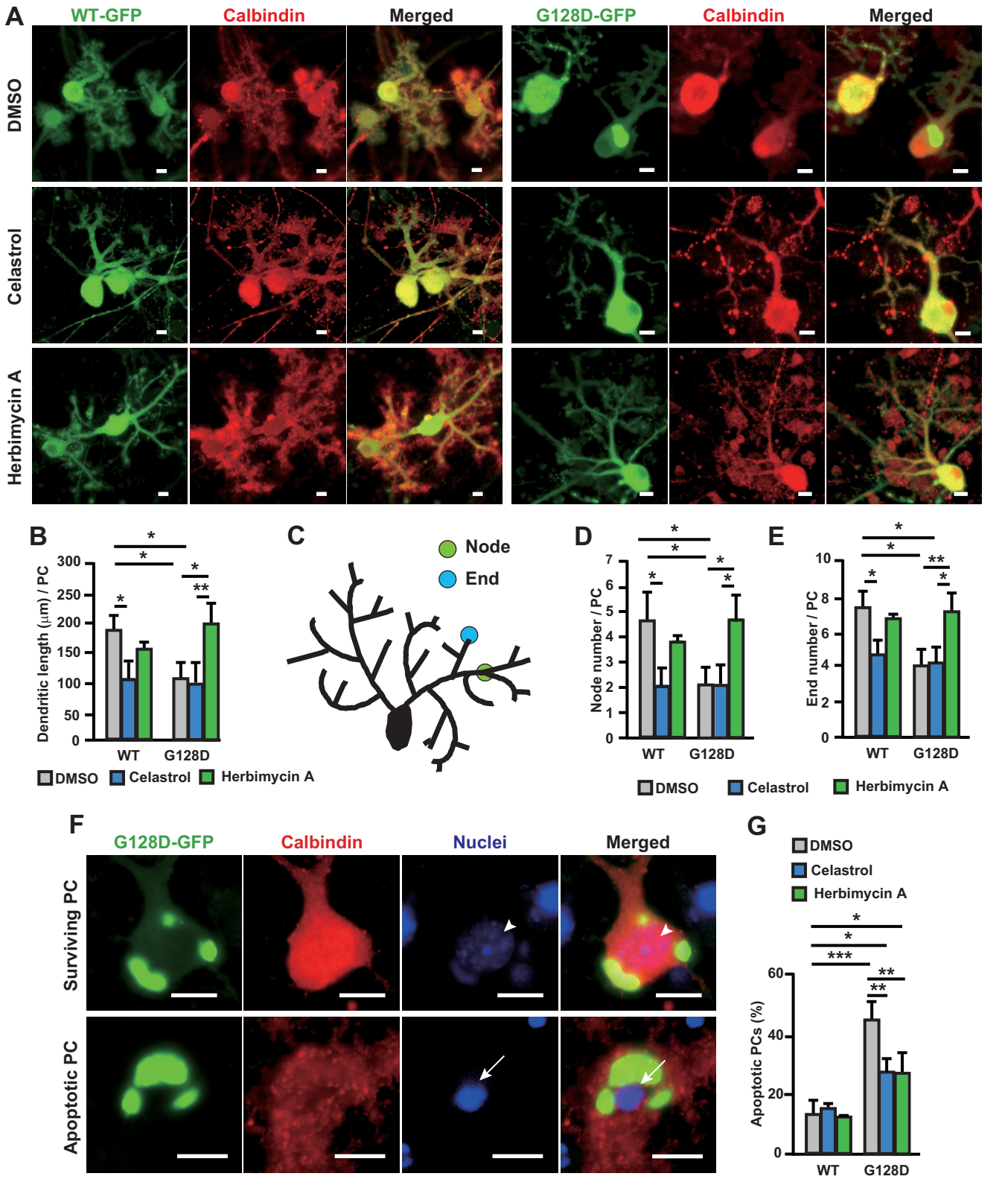

Figure 7. Pharmacological induction of Hsp70 ameliorates mutant PKCγ toxicity in primary cultured PCs. *A*, representative confocal images of PCs expressing WT or G128D PKCγ–GFP. *Scale bar* = 10 μm. *B*, quantification of total dendrite lengths per PC in *A*. Mean ± S.D., $n = 3$. *, $p < 0.05$, and **, $p < 0.01$; one-way analysis of variance with Tukey's post hoc tests. *C*, illustration of a PC showing node and end of its dendrite. *D* and *E*, quantification of number of nodes (*D*) and number of ends (*E*) per PC in *A*. Mean ± S.D., $n = 3$. *, $p < 0.05$, and **, $p < 0.01$; one-way analysis of variance with Tukey's post hoc tests. *F*, representative confocal images of apoptotic PCs expressing G128D–GFP and stained with antibodies against calbindin and Hoechst 33342. Calbindin-positive PCs with fragmented or condensed nuclei were regarded as apoptotic PCs (*arrows*); cells with normally stained nuclei were regarded as surviving PCs (*arrowheads*). *Scale bar* = 10 μm. *G*, quantitative analysis of apoptotic cells visualized by nuclear staining in *F*. Mean ± S.D., $n = 3$. *, $p < 0.05$; **, $p < 0.01$; and ***, $p < 0.001$; one-way analysis of variance with Tukey's post hoc tests.

Mechanisms alleviating cytotoxic mutant PKCγ aggregation

Exposed hydrophobic regions of misfolded proteins cause protein aggregation and are typical recognition surfaces for Hsps (22). Here, we showed that PKCγ physically interacted with Hsp70, and this interaction was enhanced by a SCA14-associated mutation. Although Hsp70 interacted with the isolated C2 as well as the kinase domain of PKCγ, the aggregation propensity of the kinase domain, calculated by the Zyggregator method, was much higher than that of the C2 domain (12). This discrepancy may be rationalized by the observation that the amino acid sequences in the C2 and kinase domains have higher intrinsic disorder propensity than those in the C1A and C1B domains. The data suggested that, when these domains are isolated, the C2 and kinase domains become unstable due to a lack of inter-domain interactions that are otherwise present in full-length PKCγ. Moreover, these domains tend to assume an unfolded structure with exposed hydrophobic regions that are recognizable by Hsp70. Conversely, WT C1A and C1B may assume globular conformations in which the hydrophobic regions are buried. Under basal conditions, full-length PKCγ displays an inactive, closed conformation; the kinase domain is masked by regulatory domains, including C1A, C1B, and C2, such that the hydrophobic regions of these domains remain inside the molecule. Upon cellular stimulation, Ca^{2+} and diacylglycerol bind the regulatory domain and induce conformational change into an open structure with exposed kinase and (potentially) C2 domains for activation (42). Although the activation of WT PKCγ is tightly regulated by these second messengers, most SCA14-associated mutants exhibit a constitutively active phenotype (10, 43, 44). Moreover, Jezierska *et al.* (11) used FRET-fluorescence lifetime imaging microscopy in living cells to verify that V138E PKCγ, a C1B domain mutant, has an exposed C terminus. These results indicate that SCA14 mutations destabilize the closed conformation of PKCγ, causing the exposure of each domain. The loss of intramolecular inter-domain interactions caused by the formation of an active open structure in SCA14-associated mutants may facilitate the binding of Hsp70 to unfolded C2 and kinase domains. Notably, Hsp70 has been previously reported to associate with the C terminus of PKCβII, an isoform of the conventional PKC; specifically, Hsp70 binds to a leucine residue that is conserved across PKCs to protect PKCβII against down-regulation (42, 45). Because this leucine residue (Leu-654) is located in the kinase domain of PKCγ, exposure of this domain caused by a SCA14-associated mutation likely uncovers one of the primary recognition sites for Hsp70. Additionally, SCA14-associated mutations in C1A or C1B decrease domain stability. The transient unfolding of C1A or C1B in mutant PKCγ increases the risk of amyloid-like aggregation, as suggested previously (12), but should also make the protein a good substrate of Hsp70. Such direct binding of Hsp70 to aggregation-prone regions in mutant C1A or C1B should effectively prevent the formation of amyloid-like aggregates.

The results show that Hsc70 was also incorporated into the PKCγ aggregates. This result is consistent with our previous report that Hsc70 was pulled down together with mutant PKCγ (46). Therefore, it is plausible that its chaperone activity could contribute to amelioration of mutant PKCγ toxicity. Hsc70 was expressed in CHO, SH-SY5Y, and primary cultured PCs. However, unlike Hsp70, Hsc70 levels were not up-regulated by mutant PKCγ; therefore, it seems that the effect of Hsc70 on aggregation is limited.

A myriad of co-chaperones and cofactors facilitate Hsp70 chaperone activity (47). Of these, Hsp40, also known as DNAJB1, is a co-chaperone that regulates the ATPase activity of Hsp70 to enable the refolding and disaggregation of misfolded proteins (30). Here, we found that the overexpression of Hsp70, combined with Hsp40, dramatically reduced PKCγ aggregation, whereas Hsp40 overexpression alone had limited effects. Although Hsp40 did not physically bind to PKCγ, it was localized to PKCγ aggregates. The J domain of Hsp40 interacts with Hsp70, suggesting that the incorporation of Hsp40 into aggregates occurred via association with Hsp70 as a co-chaperone. In contrast, Hsp105 is highly expressed in PCs (48, 49), and serves as a nucleotide exchange factor for Hsp70, but was not co-localized with aggregates in this study. Finally, neither Hsp60 nor Hsp90 co-localized with the aggregates. It is known that Hsp60 serves as a mitochondrial chaperonin (50). Although Hsp90 maintains proper protein folding in the cytoplasm (51), it did not target mutated PKCγ. Mutant PKCγ aggregates were weakly immunoreactive for Hsp27, but overexpression of this chaperone had no significant effect on aggregation. It is known that Hsp27 protects against cellular toxicity, without reducing aggregation, in several *in vitro* and *in vivo* models, including models of SCA17 (52, 53). Thus, Hsp27 may also serve a role in SCA14 pathogenesis that is independent of aggregation suppression.

The Hsps participate in protein folding, refolding of misfolded proteins, protein degradation, and disaggregation of amyloid fibrils (51, 54). They may exert cytoprotective effects in cells that express mutant PKCγs, via several pathways. We previously demonstrated that Hsp70 knockdown significantly reduced the rate of mutant PKCγ degradation and increased PKCγ protein deposition (14). Mutant PKCγ is degraded by both proteasomal and lysosomal pathways, and Hsp70 participates in both of these pathways (55). In this study, overexpression or pharmacological induction of Hsp70 improved the detergent solubility of mutant PKCγ. In both cases, monomeric forms of mutant PKCγ were significantly increased in the detergent-soluble fraction, indicating the chaperone activity of Hsps on misfolded mutant PKCγ.

Hsp90 inhibition as a potential therapeutic strategy for the treatment of SCA14

As a major transcription factor for Hsps, HSF1 is activated in response to proteotoxic stress. Recently, HSF1 was pharmacologically targeted to induce Hsps and to decrease protein aggregation and cytotoxicity in several neurodegenerative disease models (36, 38, 56, 57). Celastrol is one such compound that inhibits Hsp90 and subsequently acts as an HSF1 activator. Although the neuroprotective effects of celastrol have been demonstrated in models of amyotrophic lateral sclerosis, Alzheimer's disease, Huntington's disease, and Parkinson's disease, its effect on the cerebellum, especially PCs, was previously unclear. To the best of our knowledge, this is the first evidence

that celastrol treatment induces Hsp70 expression in the cerebellum *in vivo*, and it prevents aggregation to ameliorate cytotoxicity caused by the mutant PKCγ *in vitro*. It is possible that the celastrol-induced autophagic activity in primary cultured cerebellar cells also potentiates clearance of PKCγ aggregates, because our previous report confirmed that pharmacological activation of autophagy enhances the clearance of PKCγ aggregates (55). It has also been demonstrated that celastrol treatment reduces polyglutamine aggregation and toxicity by up-regulating Hsp70 via the activation of HSF1 in a cell culture model of Huntington's disease (36). Thus, celastrol may exert neuroprotective effects in other SCAs, such as SCA1–3, -6, -7, -12, and -17.

Herbal extracts containing celastrol have been used in traditional Chinese medicine to treat rheumatoid arthritis for many years. Purified celastrol exerts anti-inflammatory and anti-cancer effects through multiple molecular mechanisms (58). Among them, the suppression of nuclear factor κ-light-chain-enhancer of activated B cells (NF-κB) signaling is well known, and it is noteworthy that NF-κB activation is required for dendritic growth in PCs through transcriptional up-regulation of the microtubule-associated proteins, MAP2 and MAP1B (59). At the doses tested where celastrol induced Hsp70, and diminished aggregation and apoptosis in PCs expressing mutant PKCγ, the treatment failed to improve dendritic development, and it also elicited dendritic regression in PCs expressing WT PKCγ. We speculate that these effects may reflect celastrol-induced suppression of NF-κB signaling and dendritic toxicity in PCs. Additionally, celastrol exerts anti-obesity effects by increasing energy expenditure through pharmacological activation of HSF1 in mice (60, 61). We also observed similar effects of celastrol treatment on body weight; whereas the weights of DMSO-treated mice increased over the 2-week study period ($13.7 \pm 3.8\%$ (S.E. of the mean), $n = 8$), the weights of celastrol-treated mice decreased ($0.9 \pm 2.8\%$, $n = 7$). Moreover, it was reported that co-application of celastrol and arimoclomol, a co-activator of HSF1, improved the efficiency of celastrol-mediated Hsp induction (62). Thus, additional studies regarding the optimization of celastrol treatment are required for its therapeutic application against SCA.

Herbimycin A, a benzoquinone ansamycin, is also an inhibitor of Hsp90 that binds its nucleotide-binding site to activate HSF1 (63). In primary cultured PCs expressing mutant PKCγ, we found that the up-regulation of Hsp70 by herbimycin A suppressed *de novo* amyloid and amorphous aggregation of mutant PKCγ, ameliorated abnormal dendritic formation, and diminished apoptosis.

Our results indicate that aggregation of mutant PKCγ reflects a dynamic equilibrium between aggregate formation and disassembly. In both control but especially in herbimycin A-treated cells, we observed disaggregation of already formed aggregates, including relatively large aggregates (5 μm and larger). Inasmuch as herbimycin A did not potentiate autophagic activity, it seems plausible that the enhanced clearance of aggregates by herbimycin A involves Hsp70-dependent disaggregation. This role would be consistent with the observations of Gao *et al.* (54), who reported that human Hsp70 disaggregase-associated chaperone components can disassemble purified α-synuclein amyloid fibrils that are characteristic of Parkinson's disease.

We also observed that herbimycin A showed poor blood-brain barrier permeability; herbimycin A at 2 mg/kg (2-fold greater than the effective dose of celastrol) failed to induce Hsps in the mouse cerebellum. Low blood-brain barrier permeability of herbimycin A analogs, including geldanamycin and 17-(dimethylaminoethylamino)-17-demethoxygeldanamycin (17-DMAG), has been reported previously (64), and Silva-Fernandes *et al.* (65) showed that Hsp induction by 17-DMAG in the brain of SCA3 model mice required high-dose (25 mg/kg) intraperitoneal (i.p.) administration.

As described above, it is unlikely that celastrol or herbimycin will advance as drugs for SCA14, due to their toxicity and poor blood-brain barrier permeability. Recently, several novel small-molecule Hsp90 inhibitors have been developed, some of which have been demonstrated to induce brain Hsps in murine models of Alzheimer's disease and Parkinson's disease (66, 67). Furthermore, although some of these compounds have failed in clinical trials for various malignancies or cancers due to limited clinical activity, the adverse effects of the drugs were manageable (68). These compounds may be of utility as therapeutic agents against SCA14.

Experimental procedures

Chemicals and antibodies

Celastrol (219465) and PES-Cl (531067) were obtained from Calbiochem (Millipore, Darmstadt, Germany). Herbimycin A (OP12) was obtained from Kyowa Medex (Tokyo, Japan). Sources and dilutions of primary antibodies were as follows: mouse anti-Hsp27 (SPA-800, RRID: AB_10618555, 1:500), rabbit anti-Hsp40 antibody (SPA-400, RRID: AB_1505543, 1:3000 for immunoblotting and 1:300 for immunocytochemistry), mouse anti-Hsp70 antibody (SPA-810, RRID: AB_10615203, 1:1000 for immunoblotting and 1:150 for immunocytochemistry), and mouse anti-Hsp90 antibody (SPA-830, RRID: AB_2314653, 1:500) were obtained from Enzo Life Sciences (Farmingdale, NY); rabbit anti-PKCγ antibody (RRID: AB_632234, 1:1500), rabbit anti-Hsp105 antibody (sc-6241, RRID: AB_2119250, 1:50), and mouse anti-calbindin D28K antibody (sc-365360, RRID: AB_10841576, 1:200) were obtained from Santa Cruz Biotechnology (Dallas, TX); rabbit anti-calbindin D28K antibody (AB1778, RRID: AB_2068336, 1:200) was obtained from EMD-Millipore; rabbit anti-Hsp60 (D307) antibody (4870, RRID:AB_2295614, 1:100) was obtained from Cell Signaling Technology (Danvers, MA); HRP-conjugated anti-FLAG (M2) antibody (A8592, RRID: AB_439702, 1:1500) was obtained from Sigma); rat anti-Hsc70 antibody (ab19136, RRID:AB_444764, 1:1000) was obtained from Abcam (Cambridge, UK); and HRP-conjugated anti-α-tubulin antibody (PM054-7, RRID: AB_10695326, 1:1500), rabbit anti-LC3 antibody (PM036, RRID:AB_2274121, 1:1000), and anti-Myc tag antibody (M192-7, 1:10000) were obtained from MBL (Nagoya, Japan). Alexa Fluor 488- and 594-conjugated secondary antibodies (1:1000) were obtained from Invitrogen (ThermoFisher Scientific, Waltham, MA). Horseradish peroxidase-conjugated secondary antibodies (115-036-072, RRID: AB_2338525 and

111-036-045, RRID: AB_2337943, 1:5000–10000) were obtained from Jackson ImmunoResearch (West Grove, PA).

Plasmid construction

The generation of plasmids for GFP-, Myc-, or FLAG-tagged WT PKCγ, mutant PKCγ, or domains from PKCγ has been previously described (12). Plasmid constructs of Hsp40 (DNAJB1) in pRc/CMV and Hsp70 (HSPA1A) in pCMV were kindly gifted by Dr. Sobue (Nagoya University, Japan) and cloned into pcDNA3.1-Myc; K71E or T13G was introduced into Myc–Hsp70 using the QuikChange II XL site-directed mutagenesis kit (Agilent Technologies, Santa Clara, CA). Human Hsp27 (HSPB1) cDNA (GenBank™ accession no. NM_001540) was obtained by RT-PCR, as described previously (43), and cloned into pcDNA3.1-Myc. The adenoviral vectors Ad-L7–tTA, Ad-TetOp-WT PKCγ–GFP, and Ad-TetOP-G128D PKCγ–GFP were constructed as described previously (7).

Cell culture, transfection, and adenovirus infection

The SH-SY5Y, CHO, and COS-7 cells were maintained in Ham's/Dulbecco's modified Eagle's medium (DMEM) containing Glutamax, Ham, and DMEM, respectively, at 37 °C under a humidified atmosphere of 5% CO_2. All media were supplemented with 10% fetal bovine serum, 100 units/ml penicillin, and 100 μg/ml streptomycin. Transient transfection was performed with Lipofectamine 2000 (Invitrogen), Lipofectamine LTX (Invitrogen), Lipofectamine 3000 (Invitrogen), or FuGENE™ 6 (Roche Applied Science, Basel, Switzerland) for SH-SY5Y, CHO, and COS-7 cells, respectively.

Mouse cerebellar primary cultures were prepared as described previously (7). Briefly, E14 embryos from pregnant ICR mice were dissociated using Neuron Dissociation Solutions (291-78001; Wako Pure Chemical Industries, Ltd., Osaka, Japan) in accordance with the manufacturer's specifications. Dissociated cerebellar cells were suspended in neuronal culture medium (148-09671; Wako Pure Chemical Industries, Ltd.) containing triiodothyronine (100 pM, T6397; Sigma) in a polyethylenimine (0.01%, P3143; Sigma)-coated 8-well cover glass chamber (5232-008; Iwaki, AGC Techno Glass Co., Ltd., Shizuoka, Japan), glass bottom dish, or poly-L-lysine (0.1%, P8920; Sigma)-coated 24-well plate and cultured for 22–30 DIV at 37 °C under a humidified atmosphere of 5% CO_2. Half of the culture medium was replaced by fresh medium twice a week. On DIV 21, cultured cells were infected with adenoviral vectors Ad-L7–tTA (1.5×10^3 pfu/dish) and Ad-TetOp-WT-PKCγ–GFP (1.5×10^3 pfu/dish) or TetOp-G128D-PKCγ–GFP (1.0×10^3 pfu/dish).

Immunofluorescence staining, confocal imaging, and cell counting

The SH-SY5Y and CHO cells expressing the indicated recombinant proteins in glass-bottom dishes were fixed with 4% paraformaldehyde/phosphate-buffered saline (PBS) for 1 h at room temperature. After washing, the cells were incubated in 10% normal goat serum/Tris-buffered saline (TBS) containing 0.1% Tween 20 (TBS-T) for 30 min. After blocking, the cells were incubated with the appropriate primary antibodies for 2 h at room temperature or overnight at 4 °C, followed by incubation with appropriate fluorescence-tagged secondary antibodies. Immunostaining was assessed by confocal immunofluorescence microscopy (LSM700, Carl Zeiss, Germany).

The CHO and SH-SY5Y cells transfected with Hsp70 and/or PKCγ–GFP were cultured for 1–2 days and fixed, as described above. After two washes with PBS, cells were observed by confocal microscopy. A total of 200–300 GFP-positive and Hsp70-positive cells were counted.

Co-immunoprecipitation

Both co-IP and immunoblotting were performed as described previously (12). Briefly, 1 day after transfection, COS-7 cells were washed, harvested with ice-cold PBS, and resuspended in TBS-T (150 mM NaCl, 0.5% Triton X-100, and 50 mM Tris-HCl, pH 7.4) containing protease inhibitor mixture (0369-21, Nacalai Tesque, Kyoto, Japan). After homogenization with a sonicator, cell lysates were cleared by centrifugation for 15 min at 15,000 × *g* at 4 °C. The resulting supernatants were incubated for 2 h at 4 °C with anti-DDDDK-tag mAb-magnetic agarose (M185-10, MBL). Immunoprecipitates were washed at least three times with ice-cold TBS-T, mixed with 2× SDS sample buffer, and boiled for 5 min at 95 °C.

Cell death analysis

CHO cells transfected using FuGENE 6 (Promega, Madison, WI) were cultured on 6-cm diameter dishes for 2 days. Flow cytometric analyses were conducted using the FACSCalibur system (BD Biosciences) as described previously (9), with slight modifications. Briefly, we used 7-AAD (559925, BD Biosciences) as a marker for dead cells. For each sample, the fluorescence of 2×10^4 cells was recorded and analyzed by Cell Quest™ software (BD Biosciences).

Among PCs, cells with condensed or fragmented nuclei were considered to be apoptotic. The extent of apoptosis triggered by mutant PKCγ–GFP was evaluated using nuclear fluorescent Hoechst 33342 staining, as described previously (7, 13). Briefly, cultured cells (DIV 21) were transduced with adenoviral vectors Ad-L7–tTA (1.5×10^3 pfu/dish) and Ad-TetOp-WT-PKCγ–GFP (2.0×10^3 pfu/dish) or TetOp-G128D-PKCγ–GFP (2.0×10^3 pfu/dish), and the indicated drug treatments were started 5 days after infection, for a 4-day period. On DIV 30, cells were fixed with 4% paraformaldehyde in PBS, stained with 0.5 μg/ml Hoechst 33342, and subsequently stained with anti-calbindin D28K mouse mAb and Alexa594 anti-mouse IgG antibody. The fluorescence of PKCγ–GFP, Alexa Fluor 594, and Hoechst 33342 was monitored using confocal microscopy (LSM700, Carl Zeiss).

Triton X-100 solubility fractionation and immunoblotting

One day after transfection, CHO cells in 6-well plate dishes were washed, harvested with ice-cold PBS, and resuspended in 40 μl of TBS-T (150 mM NaCl, 1% Triton X-100, and 50 mM Tris-HCl, pH 7.4) containing protease inhibitor mixture. After homogenization with a sonicator, 10 μl of each cell lysate was preserved for analysis as inputs. The remaining homogenates were centrifuged for 12 min at 20,000 × *g* at 4 °C, and the resulting supernatants were collected as the Triton X-100–soluble

fraction. Supernatant protein concentrations were determined using a bicinchoninic protein assay kit (Pierce, ThermoFisher Scientific). The inputs and Triton X-100–soluble fractions were mixed with SDS sample buffer. Pellets were resuspended with 2× SDS sample buffer, sonicated, and used as the Triton X-100–insoluble fraction. The SDS sample buffer did not contain any reducing agents. All fractions were boiled for 10 min at 50 °C, and equal amounts of protein were subjected to SDS-PAGE and Western blotting. Signals were detected using the ChemiDoc XRS system (Bio-Rad), and quantitative analyses were performed using Quantity One software (Bio-Rad). All comparisons were made between bands on single blots.

All drug treatments were performed 5 h after transfection with Q127R PKCγ–GFP in SH-SY5Y cells. Celastrol (3 μM) treatment was performed for 3 h, and subsequently, the medium containing celastrol was replaced with fresh medium. After 16 h of cultivation, cells were harvested. Harvested cells were subjected to Triton X-100 solubility fractionation, as described above.

Treatment of primary cultured PCs for Western blotting

Approximately 6×10^5 mouse cerebellar primary cells were cultured in poly-L-lysine–coated 24-well dishes. On DIV 21, celastrol (3 μM, 1 h, followed by 23 h of incubation without celastrol), herbimycin A (2 μM, 24 h), or DMSO-treated primary cultured PCs were harvested with ice-cold PBS and resuspended in TBS-T containing a protease inhibitor mixture. After homogenization with a sonicator, whole-cell lysates were mixed with SDS sample buffer and boiled for 5 min at 95 °C. Quantities of 40 μg (Hsp70) and 10 μg (Hsc70/Hsp40) of protein were subjected to SDS-PAGE to quantify the expression levels of Hsps and normalized to α-tubulin. For LC3-II detection, cells were directly harvested with 60 μl of SDS sample buffer, boiled for 5 min at 95 °C, and sonicated and then 20 μl of the lysates were subjected to SDS-PAGE. Chloroquine (50 μM, 17 h; C6628, Sigma) was used to accumulate LC3-II. The LC3-II expression levels were normalized to α-tubulin.

Treatment of primary cultured PCs for fluorescence microscopy observation

To observe the pharmacological induction of endogenous Hsp70 expression in the primary cultured PCs, the cells were treated with celastrol (3 μM, 1 h/day), herbimycin A (2 μM), or DMSO for 4 days on DIV 21. The cells were fixed and stained with antibodies against Hsp70 and calbindin.

The PCs expressing WT or G128D PKCγ–GFP were treated with celastrol (3 μM, 1 h/day, for 4 days), herbimycin A (2 μM, 4 days), or DMSO. Cells were fixed and stained for calbindin and assessed by confocal microscopy. The intensity of GFP was measured, and the aggregates showing fluorescence intensity >250 a.u. were designated as high-intensity aggregates. At least 100 calbindin- and GFP-positive cells were counted per dish. Total dendrite length and total nodes or end numbers were measured using Neurolucida and Neurolucida Explorer software (MBF Bioscience, Tokyo, Japan). At least 30 calbindin- and GFP-positive cells were analyzed per dish.

Long-term time-lapse imaging

Long-term time-lapse imaging was performed using a computer-assisted fluorescent microscope, the LCV100 incubation imaging system (Olympus, Tokyo, Japan). This device possesses the ability to monitor fluorescence in living cells under normal culture conditions (37 °C, 95% humidity, and 5% CO_2). Five days after adenoviral transduction, GFP fluorescence of DMSO-treated or 2 μM herbimycin A-treated primary cultured PCs was observed for 51 h. For the experiments performed to observe the effects of Hsp70 inhibition, the cells were treated with 2 μM herbimycin A for 8 h, followed by addition of DMSO or PES-Cl (10 μM), and then the cells were observed for 46 h using the LCV100. Sequential GFP fluorescence images of PCs were obtained every 1 h and analyzed using MetaMorph software (Molecular Devices Corp.).

Pharmacological induction of Hsps in mice

All animal studies were approved by the Institutional Animal Care and Use Committee and conducted in accordance with the Kobe University Animal Experimentation Regulations. All efforts were made to minimize suffering and to reduce the number of animals used. Four-week-old male C57BL/6N mice were obtained from Japan SLC, Inc. (Shizuoka, Japan) and treated with celastrol (1 mg/kg, i.p.), herbimycin A (2 mg/kg, i.p.), or DMSO (10% DMSO in PBS, i.p.) once daily for the indicated durations. Animals were humanely euthanized, and the cerebellum was dissected out and homogenized by sonication in ice-cold TBS-T (50 mM Tris-HCl, 150 mM NaCl, 1 mM EDTA, and 1% Triton X-100, pH 7.4) containing a protease inhibitor mixture. Brain homogenates were centrifuged at 20,000 × *g* for 15 min at 4 °C. The resulting supernatants were collected, mixed with SDS sample buffer, and boiled for 5 min at 95 °C. Quantities of 10 μg (Hsp40) and 40 μg (Hsp70) of protein were subjected SDS-PAGE to quantify the expression levels of Hsps and normalized to α-tubulin.

Experimental design and statistical analysis

Two-tailed unpaired *t*-tests (to compare two groups) and one-way analyses of variance with Tukey's post hoc tests (to compare three or more groups) were conducted using Graph Pad Prism 5 (La Jolla, CA; RRID: SCR_002798). All numbers and sample sizes for each experiment are indicated in the corresponding figure legends.

Author contributions—A. N. and N. A. data curation; A. N. and N. A. formal analysis; A. N., N. A., and H. T. investigation; A. N. and H. T. writing-original draft; N. A., H. T., and N. Saito conceptualization; N. A. and N. Saito supervision; N. A. project administration; N. A. and N. Saito writing-review and editing; T. S., T. U., and N. Sakai resources; D. H. methodology; T. S. and N. Saito funding acquisition.

Acknowledgment—We thank Dr. Gen Sobue for providing the Hsp40 and Hsp70 expression plasmids.

References

1. Aguzzi, A., and O'Connor, T. (2010) Protein aggregation diseases: pathogenicity and therapeutic perspectives. *Nat. Rev. Drug Discov.* **9,** 237–248 CrossRef Medline

2. Wyttenbach, A. (2004) Role of heat shock proteins during polyglutamine neurodegeneration: mechanisms and hypothesis. *J. Mol. Neurosci.* **23,** 69–96 CrossRef Medline
3. Smeets, C. J., and Verbeek, D. S. (2016) Climbing fibers in spinocerebellar ataxia: a mechanism for the loss of motor control. *Neurobiol. Dis.* **88,** 96–106 CrossRef Medline
4. Chen, D. H., Brkanac, Z., Verlinde, C. L., Tan, X. J., Bylenok, L., Nochlin, D., Matsushita, M., Lipe, H., Wolff, J., Fernandez, M., Cimino, P. J., Bird, T. D., and Raskind, W. H. (2003) Missense mutations in the regulatory domain of PKCγ: a new mechanism for dominant nonepisodic cerebellar ataxia. *Am. J. Hum. Genet.* **72,** 839–849 CrossRef Medline
5. Saito, N., Kikkawa, U., Nishizuka, Y., and Tanaka, C. (1988) Distribution of protein kinase C-like immunoreactive neurons in rat brain. *J. Neurosci.* **8,** 369–382 CrossRef Medline
6. Kose, A., Saito, N., Ito, H., Kikkawa, U., Nishizuka, Y., and Tanaka, C. (1988) Electron microscopic localization of type I protein kinase C in rat Purkinje cells. *J. Neurosci.* **8,** 4262–4268 CrossRef Medline
7. Seki, T., Shimahara, T., Yamamoto, K., Abe, N., Amano, T., Adachi, N., Takahashi, H., Kashiwagi, K., Saito, N., and Sakai, N. (2009) Mutant γPKC found in spinocerebellar ataxia type 14 induces aggregate-independent maldevelopment of dendrites in primary cultured Purkinje cells. *Neurobiol. Dis.* **33,** 260–273 CrossRef Medline
8. Shuvaev, A. N., Horiuchi, H., Seki, T., Goenawan, H., Irie, T., Iizuka, A., Sakai, N., and Hirai, H. (2011) Mutant PKCγ in spinocerebellar ataxia type 14 disrupts synapse elimination and long-term depression in Purkinje cells *in vivo*. *J. Neurosci.* **31,** 14324–14334 CrossRef Medline
9. Seki, T., Adachi, N., Ono, Y., Mochizuki, H., Hiramoto, K., Amano, T., Matsubayashi, H., Matsumoto, M., Kawakami, H., Saito, N., and Sakai, N. (2005) Mutant protein kinase Cγ found in spinocerebellar ataxia type 14 is susceptible to aggregation and causes cell death. *J. Biol. Chem.* **280,** 29096–29106 CrossRef Medline
10. Asai, H., Hirano, M., Shimada, K., Kiriyama, T., Furiya, Y., Ikeda, M., Iwamoto, T., Mori, T., Nishinaka, K., Konishi, N., Udaka, F., and Ueno, S. (2009) Protein kinase Cγ, a protein causative for dominant ataxia, negatively regulates nuclear import of recessive-ataxia-related aprataxin. *Hum. Mol. Genet.* **18,** 3533–3543 CrossRef Medline
11. Jezierska, J., Goedhart, J., Kampinga, H. H., Reits, E. A., and Verbeek, D. S. (2014) SCA14 mutation V138E leads to partly unfolded PKCγ associated with an exposed C terminus, altered kinetics, phosphorylation and enhanced insolubilization. *J. Neurochem.* **128,** 741–751 CrossRef Medline
12. Takahashi, H., Adachi, N., Shirafuji, T., Danno, S., Ueyama, T., Vendruscolo, M., Shuvaev, A. N., Sugimoto, T., Seki, T., Hamada, D., Irie, K., Hirai, H., Sakai, N., and Saito, N. (2015) Identification and characterization of PKCγ, a kinase associated with SCA14, as an amyloidogenic protein. *Hum. Mol. Genet.* **24,** 525–539 CrossRef Medline
13. Seki, T., Takahashi, H., Yamamoto, K., Ogawa, K., Onji, T., Adachi, N., Tanaka, S., Hide, I., Saito, N., and Sakai, N. (2010) Congo red, an amyloid-inhibiting compound, alleviates various types of cellular dysfunction triggered by mutant protein kinase Cγ that causes spinocerebellar ataxia type 14 (SCA14) by inhibiting oligomerization and aggregation. *J. Pharmacol. Sci.* **114,** 206–216 CrossRef Medline
14. Ogawa, K., Seki, T., Onji, T., Adachi, N., Tanaka, S., Hide, I., Saito, N., and Sakai, N. (2013) Mutant γPKC that causes spinocerebellar ataxia type 14 upregulates Hsp70, which protects cells from the mutant's cytotoxicity. *Biochem. Biophys. Res. Commun.* **440,** 25–30 CrossRef Medline
15. Ganos, C., Zittel, S., Minnerop, M., Schunke, O., Heinbokel, C., Gerloff, C., Zühlke, C., Bauer, P., Klockgether, T., Münchau, A., and Bäumer, T. (2014) Clinical and neurophysiological profile of four German families with spinocerebellar ataxia type 14. *Cerebellum* **13,** 89–96 CrossRef Medline
16. Koht, J., Stevanin, G., Durr, A., Mundwiller, E., Brice, A., and Tallaksen, C. M. (2012) SCA14 in Norway, two families with autosomal dominant cerebellar ataxia and a novel mutation in the PRKCG gene. *Acta Neurol. Scand.* **125,** 116–122 CrossRef Medline
17. Sailer, A., Scholz, S. W., Gibbs, J. R., Tucci, A., Johnson, J. O., Wood, N. W., Plagnol, V., Hummerich, H., Ding, J., Hernandez, D., Hardy, J., Federoff, H. J., Traynor, B. J., Singleton, A. B., and Houlden, H. (2012) Exome sequencing in an SCA14 family demonstrates its utility in diagnosing heterogeneous diseases. *Neurology* **79,** 127–131 CrossRef Medline
18. Seki, T., Adachi, N., Abe-Seki, N., Shimahara, T., Takahashi, H., Yamamoto, K., Saito, N., and Sakai, N. (2011) Elucidation of the molecular mechanism and exploration of novel therapeutics for spinocerebellar ataxia caused by mutant protein kinase Cγ. *J. Pharmacol. Sci.* **116,** 239–247 CrossRef Medline
19. Ueda, T., Seki, T., Katanazaka, K., Sekiguchi, K., Kobayashi, K., Kanda, F., and Toda, T. (2013) A novel mutation in the C2 domain of protein kinase Cγ associated with spinocerebellar ataxia type 14. *J. Neurol.* **260,** 1664–1666 CrossRef Medline
20. van Gaalen, J., Vermeer, S., van Veluw, M., van de Warrenburg, B. P., and Dooijes, D. (2013) A *de novo* SCA14 mutation in an isolated case of late-onset cerebellar ataxia. *Mov. Disord.* **28,** 1902–1903 CrossRef Medline
21. Seki, T., Abe-Seki, N., Kikawada, T., Takahashi, H., Yamamoto, K., Adachi, N., Tanaka, S., Hide, I., Saito, N., and Sakai, N. (2010) Effect of trehalose on the properties of mutant γPKC, which causes spinocerebellar ataxia type 14, in neuronal cell lines and cultured Purkinje cells. *J. Biol. Chem.* **285,** 33252–33264 CrossRef Medline
22. Clerico, E. M., Tilitsky, J. M., Meng, W., and Gierasch, L. M. (2015) How hsp70 molecular machines interact with their substrates to mediate diverse physiological functions. *J. Mol. Biol.* **427,** 1575–1588 CrossRef Medline
23. Dosztányi, Z., Csizmok, V., Tompa, P., and Simon, I. (2005) IUPred: web server for the prediction of intrinsically unstructured regions of proteins based on estimated energy content. *Bioinformatics* **21,** 3433–3434 CrossRef Medline
24. Dosztányi, Z., Csizmók, V., Tompa, P., and Simon, I. (2005) The pairwise energy content estimated from amino acid composition discriminates between folded and intrinsically unstructured proteins. *J. Mol. Biol.* **347,** 827–839 CrossRef Medline
25. Levy, J. R., Sumner, C. J., Caviston, J. P., Tokito, M. K., Ranganathan, S., Ligon, L. A., Wallace, K. E., LaMonte, B. H., Harmison, G. G., Puls, I., Fischbeck, K. H., and Holzbaur, E. L. (2006) A motor neuron disease-associated mutation in p150Glued perturbs dynactin function and induces protein aggregation. *J. Cell Biol.* **172,** 733–745 CrossRef Medline
26. Sousa, M. C., and McKay, D. B. (1998) The hydroxyl of threonine 13 of the bovine 70-kDa heat shock cognate protein is essential for transducing the ATP-induced conformational change. *Biochemistry* **37,** 15392–15399 CrossRef Medline
27. Bilen, J., and Bonini, N. M. (2007) Genome-wide screen for modifiers of ataxin-3 neurodegeneration in *Drosophila*. *PLoS Genet.* **3,** 1950–1964 Medline
28. Schmid, I., Krall, W. J., Uittenbogaart, C. H., Braun, J., and Giorgi, J. V. (1992) Dead cell discrimination with 7-amino-actinomycin D in combination with dual color immunofluorescence in single laser flow cytometry. *Cytometry* **13,** 204–208 CrossRef Medline
29. Divya, T., Sureshkumar, A., and Sudhandiran, G. (2017) Autophagy induction by celastrol augments protection against bleomycin-induced experimental pulmonary fibrosis in rats: Role of adaptor protein p62/ SQSTM1. *Pulm. Pharmacol. Ther.* **45,** 47–61 CrossRef Medline
30. Fan, C. Y., Lee, S., and Cyr, D. M. (2003) Mechanisms for regulation of Hsp70 function by Hsp40. *Cell Stress Chaperones* **8,** 309–316 CrossRef Medline
31. Waelter, S., Boeddrich, A., Lurz, R., Scherzinger, E., Lueder, G., Lehrach, H., and Wanker, E. E. (2001) Accumulation of mutant huntingtin fragments in aggresome-like inclusion bodies as a result of insufficient protein degradation. *Mol. Biol. Cell* **12,** 1393–1407 CrossRef Medline
32. DeTure, M., Ko, L. W., Easson, C., and Yen, S. H. (2002) Tau assembly in inducible transfectants expressing wild-type or FTDP-17 tau. *Am. J. Pathol.* **161,** 1711–1722 CrossRef Medline
33. Klucken, J., Shin, Y., Masliah, E., Hyman, B. T., and McLean, P. J. (2004) Hsp70 reduces α-synuclein aggregation and toxicity. *J. Biol. Chem.* **279,** 25497–25502 CrossRef Medline
34. Westerheide, S. D., Bosman, J. D., Mbadugha, B. N., Kawahara, T. L., Matsumoto, G., Kim, S., Gu, W., Devlin, J. P., Silverman, R. B., and Morimoto, R. I. (2004) Celastrols as inducers of the heat shock response and cytoprotection. *J. Biol. Chem.* **279,** 56053–56060 CrossRef Medline

35. Zhang, T., Hamza, A., Cao, X., Wang, B., Yu, S., Zhan, C. G., and Sun, D. (2008) A novel Hsp90 inhibitor to disrupt Hsp90/Cdc37 complex against pancreatic cancer cells. *Mol. Cancer Ther.* **7,** 162–170 CrossRef Medline
36. Zhang, Y. Q., and Sarge, K. D. (2007) Celastrol inhibits polyglutamine aggregation and toxicity through induction of the heat shock response. *J. Mol. Med.* **85,** 1421–1428 CrossRef Medline
37. Hamel, L., Kenney, M., Jayyosi, Z., Ardati, A., Clark, K., Spada, A., Zilberstein, A., Perrone, M., Kaplow, J., Merkel, L., and Rojas, C. (2000) Induction of heat shock protein 70 by herbimycin A and cyclopentenone prostaglandins in smooth muscle cells. *Cell Stress Chaperones* **5,** 121–131 CrossRef Medline
38. Paris, D., Ganey, N. J., Laporte, V., Patel, N. S., Beaulieu-Abdelahad, D., Bachmeier, C., March, A., Ait-Ghezala, G., and Mullan, M. J. (2010) Reduction of β-amyloid pathology by celastrol in a transgenic mouse model of Alzheimer's disease. *J. Neuroinflammation* **7,** 17 CrossRef Medline
39. Deng, Y. N., Shi, J., Liu, J., and Qu, Q. M. (2013) Celastrol protects human neuroblastoma SH-SY5Y cells from rotenone-induced injury through induction of autophagy. *Neurochem. Int.* **63,** 1–9 CrossRef Medline
40. Guo, J., Huang, X., Wang, H., and Yang, H. (2015) Celastrol induces autophagy by targeting AR/miR-101 in prostate cancer cells. *PLoS ONE* **10,** e0140745 CrossRef Medline
41. Tanida, I., Ueno, T., and Kominami, E. (2008) LC3 and autophagy. *Methods Mol. Biol.* **445,** 77–88 CrossRef Medline
42. Newton, A. C. (2003) Regulation of the ABC kinases by phosphorylation: protein kinase C as a paradigm. *Biochem. J.* **370,** 361–371 CrossRef Medline
43. Adachi, N., Kobayashi, T., Takahashi, H., Kawasaki, T., Shirai, Y., Ueyama, T., Matsuda, T., Seki, T., Sakai, N., and Saito, N. (2008) Enzymological analysis of mutant protein kinase Cγ causing spinocerebellar ataxia type 14 and dysfunction in Ca^{2+} homeostasis. *J. Biol. Chem.* **283,** 19854–19863 CrossRef Medline
44. Verbeek, D. S., Knight, M. A., Harmison, G. G., Fischbeck, K. H., and Howell, B. W. (2005) Protein kinase Cγ mutations in spinocerebellar ataxia 14 increase kinase activity and alter membrane targeting. *Brain* **128,** 436–442 Medline
45. Gao, T., and Newton, A. C. (2002) The turn motif is a phosphorylation switch that regulates the binding of Hsp70 to protein kinase C. *J. Biol. Chem.* **277,** 31585–31592 CrossRef Medline
46. Seki, T., Yoshino, K. I., Tanaka, S., Dohi, E., Onji, T., Yamamoto, K., Hide, I., Paulson, H. L., Saito, N., and Sakai, N. (2012) Establishment of a novel fluorescence-based method to evaluate chaperone-mediated autophagy in a single neuron. *PLoS ONE* **7,** e31232 CrossRef Medline
47. Mayer, M. P., and Bukau, B. (2005) Hsp70 chaperones: cellular functions and molecular mechanism. *Cell. Mol. Life Sci.* **62,** 670–684 CrossRef Medline
48. Easton, D. P., Kaneko, Y., and Subjeck, J. R. (2000) The hsp110 and Grp1 70 stress proteins: newly recognized relatives of the Hsp70s. *Cell Stress Chaperones* **5,** 276–290 CrossRef Medline
49. Hylander, B. L., Chen, X., Graf, P. C., and Subjeck, J. R. (2000) The distribution and localization of hsp110 in brain. *Brain Res.* **869,** 49–55 CrossRef Medline
50. Gupta, R. S. (1995) Evolution of the chaperonin families (Hsp60, Hsp10 and Tcp-1) of proteins and the origin of eukaryotic cells. *Mol. Microbiol.* **15,** 1–11 CrossRef Medline
51. Kim, Y. E., Hipp, M. S., Bracher, A., Hayer-Hartl, M., and Hartl, F. U. (2013) Molecular chaperone functions in protein folding and proteostasis. *Annu. Rev. Biochem.* **82,** 323–355 CrossRef Medline
52. Friedman, M. J., Shah, A. G., Fang, Z. H., Ward, E. G., Warren, S. T., Li, S., and Li, X. J. (2007) Polyglutamine domain modulates the TBP-TFIIB interaction: implications for its normal function and neurodegeneration. *Nat. Neurosci.* **10,** 1519–1528 CrossRef Medline
53. Wyttenbach, A., Sauvageot, O., Carmichael, J., Diaz-Latoud, C., Arrigo, A. P., and Rubinsztein, D. C. (2002) Heat shock protein 27 prevents cellular polyglutamine toxicity and suppresses the increase of reactive oxygen species caused by huntingtin. *Hum. Mol. Genet.* **11,** 1137–1151 CrossRef Medline
54. Gao, X., Carroni, M., Nussbaum-Krammer, C., Mogk, A., Nillegoda, N. B., Szlachcic, A., Guilbride, D. L., Saibil, H. R., Mayer, M. P., and Bukau, B. (2015) Human Hsp70 disaggregase reverses Parkinson's-linked α-synuclein amyloid fibrils. *Mol. Cell* **59,** 781–793 CrossRef Medline
55. Yamamoto, K., Seki, T., Adachi, N., Takahashi, T., Tanaka, S., Hide, I., Saito, N., and Sakai, N. (2010) Mutant protein kinase Cγ that causes spinocerebellar ataxia type 14 (SCA14) is selectively degraded by autophagy. *Genes Cells* **15,** 425–438 Medline
56. Neef, D. W., Jaeger, A. M., and Thiele, D. J. (2011) Heat shock transcription factor 1 as a therapeutic target in neurodegenerative diseases. *Nat. Rev. Drug. Discov.* **10,** 930–944 CrossRef Medline
57. Kalmar, B., and Greensmith, L. (2009) Activation of the heat shock response in a primary cellular model of motoneuron neurodegeneration-evidence for neuroprotective and neurotoxic effects. *Cell. Mol. Biol. Lett.* **14,** 319–335 Medline
58. Cascao, R., Fonseca, J. E., and Moita, L. F. (2017) Celastrol: a spectrum of treatment opportunities in chronic diseases. *Front. Med.* **4,** 69 CrossRef Medline
59. Li, J., Gu, X., Ma, Y., Calicchio, M. L., Kong, D., Teng, Y. D., Yu, L., Crain, A. M., Vartanian, T. K., Pasqualini, R., Arap, W., Libermann, T. A., Snyder, E. Y., and Sidman, R. L. (2010) Nna1 mediates Purkinje cell dendritic development via lysyl oxidase propeptide and NF-κB signaling. *Neuron* **68,** 45–60 CrossRef Medline
60. Liu, J., Lee, J., Salazar Hernandez, M. A., Mazitschek, R., and Ozcan, U. (2015) Treatment of obesity with celastrol. *Cell* **161,** 999–1011 CrossRef Medline
61. Ma, X., Xu, L., Alberobello, A. T., Gavrilova, O., Bagattin, A., Skarulis, M., Liu, J., Finkel, T., and Mueller, E. (2015) Celastrol protects against obesity and metabolic dysfunction through activation of a HSF1-PGC1α transcriptional axis. *Cell Metab.* **22,** 695–708 CrossRef Medline
62. Deane, C. A., and Brown, I. R. (2016) Induction of heat shock proteins in differentiated human neuronal cells following co-application of celastrol and arimoclomol. *Cell Stress Chaperones* **21,** 837–848 CrossRef Medline
63. Duncan, R. F. (2005) Inhibition of Hsp90 function delays and impairs recovery from heat shock. *FEBS J.* **272,** 5244–5256 CrossRef Medline
64. Shen, H. Y., He, J. C., Wang, Y., Huang, Q. Y., and Chen, J. F. (2005) Geldanamycin induces heat shock protein 70 and protects against MPTP-induced dopaminergic neurotoxicity in mice. *J. Biol. Chem.* **280,** 39962–39969 CrossRef Medline
65. Silva-Fernandes, A., Duarte-Silva, S., Neves-Carvalho, A., Amorim, M., Soares-Cunha, C., Oliveira, P., Thirstrup, K., Teixeira-Castro, A., and Maciel, P. (2014) Chronic treatment with 17-DMAG improves balance and coordination in a new mouse model of Machado-Joseph disease. *Neurotherapeutics* **11,** 433–449 CrossRef Medline
66. Luo, W., Dou, F., Rodina, A., Chip, S., Kim, J., Zhao, Q., Moulick, K., Aguirre, J., Wu, N., Greengard, P., and Chiosis, G. (2007) Roles of heat-shock protein 90 in maintaining and facilitating the neurodegenerative phenotype in tauopathies. *Proc. Natl. Acad. Sci. U.S.A.* **104,** 9511–9516 CrossRef Medline
67. McFarland, N. R., Dimant, H., Kibuuka, L., Ebrahimi-Fakhari, D., Desjardins, C. A., Danzer, K. M., Danzer, M., Fan, Z., Schwarzschild, M. A., Hirst, W., and McLean, P. J. (2014) Chronic treatment with novel small molecule Hsp90 inhibitors rescues striatal dopamine levels but not α-synuclein-induced neuronal cell loss. *PLoS ONE* **9,** e86048 CrossRef Medline
68. Isambert, N., Delord, J. P., Soria, J. C., Hollebecque, A., Gomez-Roca, C., Purcea, D., Rouits, E., Belli, R., and Fumoleau, P. (2015) Debio0932, a second-generation oral heat shock protein (HSP) inhibitor, in patients with advanced cancer-results of a first-in-man dose-escalation study with a fixed-dose extension phase. *Ann. Oncol.* **26,** 1005–1011 CrossRef Medline